

N₂-COMPATIBLE NICKEL PRECURSOR AND HIGHLY ACTIVE WATER-OXIDATION IRIIDIUM CATALYST PREPARED BY MOCVD

トラン, ビエット, ハ

<https://doi.org/10.15017/1543951>

出版情報：九州大学, 2015, 博士（工学）, 課程博士
バージョン：
権利関係：全文ファイル公表済



**KYUSHU UNIVERSITY
GRADUATE SCHOOL OF ENGINEERING
DEPARTMENT OF CHEMISTRY AND BIOCHEMISTRY**

**N₂-COMPATIBLE NICKEL PRECURSOR AND
HIGHLY ACTIVE WATER-OXIDATION IRIIDIUM
CATALYST PREPARED BY MOCVD**

**TRAN VIET HA
2015, JUNE**

CONTENTS

Chapter 1. General introduction	1
1.1. Introduction	1
1.2. Arrangement of dissertation	3
References	4
Chapter 2. An N₂-compatible Ni⁰ metal organic chemical vapor deposition (MOCVD) precursor	6
Abstract	6
2.1. Introduction	8
2.1.1. Importance of nickel film	8
2.1.2. Previous work and obstacles	9
2.1.3 Strategy to resolve the obstacles	12
2.2. Results and discussion	14
2.2.1. Synthesis and characterization of a novel Ni ⁰ complex 1	14
2.2.2. Physical properties of complex 1	19
2.2.3. Deposition and characterization of Ni film	20
2.3. Conclusions	26
2.4. Experimental	27
2.4.1. Materials and methods	27
2.4.2. Synthesis of Ni ⁰ complex 1	28
2.4.3. Deposition of Ni film from complex 1	29
References	30

Chapter 3. An IrSi oxide film as a highly active water-oxidation catalyst	
in acidic media	32
Abstract	32
3.1. Introduction	34
3.1.1. Electrochemical water-oxidation catalyst	34
3.1.2. Previous work and obstacles	36
3.1.3. Strategy to resolve the obstacles	38
3.2. Results and discussion	40
3.2.1. Thermal properties of precursor 2	40
3.2.2. Preparation and characterization of IrSi oxide film	41
3.2.3. Electrochemical behaviors of IrSi oxide film	51
3.3. Conclusion	58
3.4. Experimental	59
3.4.1. Materials and methods	59
3.4.2. Thermal properties of precursor 2	60
3.4.3. Preparation of the IrSi oxide catalyst	60
3.4.4. Preparation of Ir oxide to compare with film F₂	61
3.4.5. Evaluation of electrochemical water-oxidation	61
References	68
 Chapter 4. Concluding remarks	 71
 Publications	 73
 Acknowledgements	 74

CHAPTER 1

GENERAL INTRODUCTION

1.1. INTRODUCTION

The metal and metal-based thin films on a substrate have been an interest because of their potential applications in many fields containing electronics and catalysis. These films have been deposited by several methods such as electro-deposition, sputtering, physical vapor deposition...etc.¹ However metal organic chemical vapor deposition (MOCVD) is considered as the most convenient way providing films with good coverage and fine structure.^{1,2} The success of this method strongly depends on the available of precursors having high volatility, reasonable thermal stability and clean decomposition. Therefore, the synthesis of new precursors or the selection of the available precursors is remarkably important and challenging to the chemists. In this dissertation, the author gives two examples of synthesis and selection of suitable MOCVD precursor to deposit metal and metal-based thin films for specific applications.

Nickel (Ni) film is very important in several fields especially in microelectronic devices.⁵ Because of some critical requirements such as conformal and uniform deposition in high aspect ratio, such Ni films have been deposited by MOCVD. However, there has not yet been any MOCVD precursor that can form high purity Ni

film using cheap and safe nitrogen (N_2) as the carrier gas, so far. In this dissertation, author attempts to synthesize a novel Ni MOCVD precursor that is able to deposit high purity Ni film using N_2 as the carrier gas.

Iridium (Ir) oxides are the best catalysts for electrochemical water-oxidation in acidic regime in terms of high catalytic activity and long-term stability.⁶ But Ir is very expensive and scarce, which hinders Ir from its applications.⁶ Some oxides such as tantalum (Ta) and tin (Sn) oxides have been doped into Ir oxide to reduce the Ir contents as well as improve catalytic ability and stability due to the synergistic interaction of multicomponent by forming solid solution of mixed metal oxides.⁷ On the other hand, silicon (Si) oxide-doped films are attractive because Si oxide is abundant. It has been used as support for many catalysts.⁸ However, it has not yet been possible to improve the activity and stability of Ir oxide-based water oxidation catalyst by doing SiO_2 .⁹ In this dissertation, author attempts to dope Si oxide into Ir oxide by MOCVD method using an iridium-silyl complex as a single precursor. This approach is expected to enhance the catalytic activity and stability as well as reduce the Ir contents in anode.

1.2. ARRANGEMENT OF DISSERTATION

This dissertation contains four chapters. Each of which discusses a specific subject. The detailed content is as follows:

In chapter 1, the author presents the importance of metal and metal-based thin film and introduces some advantages of MOCVD method to deposit these films.

In chapter 2, a novel nickel complex was designed and synthesized to satisfy the requirement of a Ni MOCVD precursor that is able to deposit a high purity Ni film using cheap and safe N_2 as the carrier gas.

In chapter 3, an IrSi oxide film was prepared by MOCVD using an iridium-silyl complex as precursor. This film exhibits highly active and stable water-oxidation catalyst in acidic condition.

In chapter 4, the author gives some conclusions and remarks of the work that has been accomplished in this dissertation.

The description and arrangement of this work is depicted in Figure 1.1.

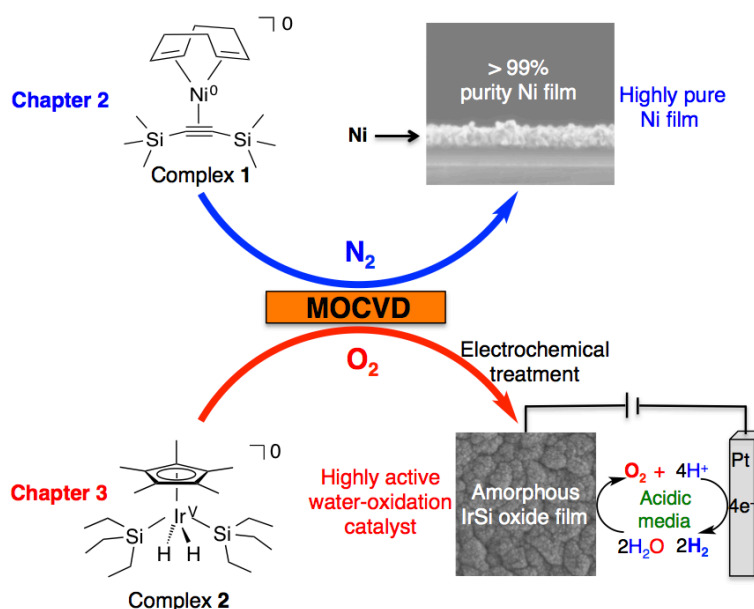


Figure 1.1 A schematic description and arrangement of this dissertation

REFERENCES

1. A. C. Jones and M. L. Hichman, *Chemical Vapour Deposition: Precursor, Process and Applications*, RSC Publishing, Cambridge 2008
2. H. Lang and S. Dietrich, *Metal-Gas-Phase Deposition and Applications, Comprehensive Inorganic Chemistry II*, Elsevier, Amsterdam 2013, 211–269.
3. A. Devi, *Coord. Chem. Rev.*, 2013, **267**, 3332–3384; N. Bahlawane, K. Kohse-Höinghaus, P. A. Premkumar and D. Lenoble, *Chem. Sci.*, 2012, **3**, 929–941; D. J.H. Emslie, P. Chadha and J. S. Price, *Coord. Chem. Rev.*, 2013, **257**, 3282–3296.
4. P. Marchand, J. A. Hassan, I. P. Parkin and C. J. Carmalt, *Danton. Trans.*, 2013, **42**, 9406–9422
5. (a) M. J. Kenney, M. Gong, Y. Li, J. Z. Wu, J. Feng, M. Lanza and H. Dai, *Science*, 2013, **342**, 836–840; (b) P. A. Premkumar, A. Dasgupta, P. Kuppusami, P. Parameswaran, C. Mallika, K. S. Nagaraja and V. S. Raghunathan, *Chem. Vap. Deposition*, 2006, **12**, 39–45.
6. (a) I. Katsounaros, S. Cherevko, A. R. Zeradjanin and K. J. J. Mayrhofer, *Angew. Chem. Int. Ed.*, 2014, **53**, 102–121; (b) E. Antolini, *ACS Catal.*, 2014, **4**, 1426–1440; (c) J. R. McKone, N. S. Lewis and H. B. Gray, *Chem. Mater.*, 2014, **26**, 407–414; (d) M. Carmo, D. L. Fritz, J. Mergel and D. Stolten, *Int. J. Hydrogen Energy*, 2013, **38**, 4901–4934; (e) S. Park, Y. Shao, J. Liu and Y. Wang, *Energy Environ. Sci.*, 2012, **5**, 9331–9344.
7. (a) Z. Yan, Y. Zhao, Z. Zhang, G. Li, H. Li, J. Wang, Z. Feng, M. Tang, X. Yuan, R. Zhang and Y. Du, *Electrochim. Acta*, 2015, **157**, 345–350; (b) J. Xu, G. Liu, J. Li and X. Wang, *Electrochim. Acta*, 2012, **59**, 105–112; (c) A. D. Blasi, C. D’Urso, V. Baglio, V. Antonucci, A. S. Arico, R. Ornelas, F.

- Matteucci, G. Orozco, D. Beltran, Y. Meas and L. G. Arriaga, *J. Appl. Electrochem.*, 2009, **39**, 191–196; (d) D. Profeti, T. A. F. Lassali and P. Olivi, *J. Appl. Electrochem.*, 2006, **36**, 883–888; (e) J.–M. Hu and J.–Q. Zhang, *J. Mater. Sci.*, 2003, **38**, 705–712; (f) C. P. De Pauli and S. Trasatti, *J. Electroanal. Chem.*, 2002, **538–539**, 145–151; (g) X. Chen, G. Chen and P. L. Yue, *J. Phys. Chem. B*, 2001, **105**, 4623–4628.
8. (a) S. Ryoji, O. Masaaki, K. Hideki and M. Hiroshi, *Bull. Chem. Soc. Jpn*, 2010, **83**, 732–734; (b) S. Nassreddine, G. Bergeret, B. Geantet and L. Piccolo, *Phys. Chem. Chem. Phys.*, 2010, **12**, 7812–7820; (c) M. Hara, J. T. Lean and T. E. Mallouk, *Chem. Matter.*, 2001, **13**, 4668–4675.
9. (a) J.–J. Zhang, J.–M. Hu, J.–Q. Zhang and C.–N. Cao, *Int. J. Hydrogen Energy*, 2011, **36**, 5218–5226; (b) X.–M. Wang, J.–M. Hu and J.–Q. Zhang, *Electrochim. Acta*, 2010, **55**, 4587–4593.

CHAPTER 2

AN N₂-COMPATIBLE Ni⁰ METAL ORGANIC CHEMICAL VAPOR DEPOSITION (MOCVD) PRECURSOR

ABSTRACT

This work describes the synthesis and characterization of a novel zero-valent nickel organometallic compound: [Ni⁰(COD)(L)] {Complex **1**, COD = 1,5-cyclooctadiene, L = 1,2-bis(trimethylsilyl)acetylene} (Figure 2.1). This complex is the first example of a Ni⁰ precursor that can deposit highly pure nickel film by metal-organic chemical vapor deposition (MOCVD) using nitrogen (N₂) as carrier gas. The volatile Ni⁰ complex was prepared conveniently in high yield from commercial-available reagents. Complex **1** was characterized by X-ray analysis, ¹H, ¹³C{¹H} NMR spectroscopies and elemental analysis to clarify the structure. The physical properties were investigated and the results demonstrated that **1** is suitable as a MOCVD precursor. The highly pure Ni film was obtained by MOCVD at low temperature deposition using cheap and safe N₂ gas as the carrier gas. Several measurements were conducted to confirm the morphology and other physical properties of the deposited Ni film. The obtained results show that the Ni⁰

organometallic complex will be a promising new MOCVD precursor for deposition of Ni film.

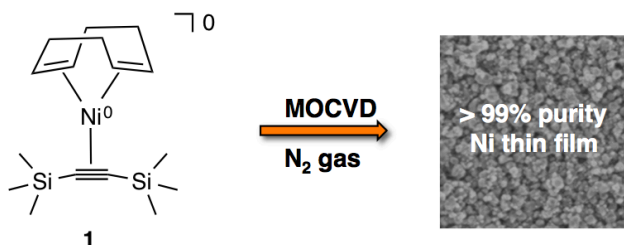


Figure 2.1 A novel zero-valent nickel organometallic compound:

$[\text{Ni}^0(\text{COD})(\text{L})]$ {**1**, COD = 1,5-cyclooctadiene, L = 1,2-bis(trimethylsilyl)acetylene}

2.1. INTRODUCTION

2.1.1. Importance of nickel film

Nickel (Ni) film has been received significant interest for various applications. Due to its excellent optical, magnetic and electrical properties, Ni film has been used in many fields.¹⁻⁷ For instance; Ni film is used for enhancement of ferrites, microelectronic devices, decorative and protective coating, selective absorbers and catalysts. Ni has also been alloyed with other elements to form novel materials. For example, nickel phosphide (Ni_2P) is an n-type semiconductor that can apply for solar cell whereas nickel sulfides are known as p-type semiconductor and nickel nitride is widely used as conductor. In addition, Ni is employed in giant magnetoresistance and memory storage devices together with cobalt. Furthermore, nickel oxides (NiO_x) can be applied to p-type transparent conducting films, chemical sensors and random access memory (RAM) ...etc.

Among the Ni-based materials, nickel silicide (NiSi) has been received the most attention because it is considered as the best material for source and drain contacts in semiconductor devices. This material is expected to replace poly-silicon gates in complementary metal-oxide silicon (CMOS) devices.^{4a} NiSi has been made by silicadation. First, a thin Ni film is deposited on a Si substrate and then is heated at high temperature. The thin NiSi film is formed by diffusion-mediated solid-state reactions between the deposited Ni film and the Si substrate. In order to grow a high quality NiSi film that can satisfy the requirement of today's electronic technology, the Ni thin film should be deposited with high purity and good conformal step coverage.

Conventionally, Ni films have been deposited by numerous methods including sputtering, pulsed laser deposition, laser ablation, physical vapor deposition (PVD), sol-gel and electro-deposition.^{4a-c} However, these methods have some drawbacks, for example, poor step coverage in high aspect ratio, high pressure and temperature

deposition. The wet-chemistry approaches such as sol-gel and electro-deposition are not suitable for semiconductor and electronic devices. The vapor phase physical methods such as, sputtering and PVD are desirable but they often suffer from poor coverage and require high temperature and vacuum.

Among the deposition methods, metal organic vapor deposition (MOCVD) is considered as the best method because it provides the potential for larger area growth, high film uniformity and especially, it offers excellent conformal step coverage on complex substrates such as narrow holes and three-dimensional structured devices.

2.1.2. Previous work and obstacles

Precursor plays a very important role in MOCVD process. The success of MOCVD strongly depends on the availability of precursors having high volatility, reasonable thermal stability and clean decomposition. Several Ni compounds have been utilized as MOCVD precursors. They can be categorized into two groups: two-valent nickel (Ni^{II}) and zero-valent nickel (Ni^0) compounds. To date, a great number of Ni^{II} MOCVD precursors have been developed, whereas Ni^0 complexes are scarce.

Tetracarbonyl nickel $\text{Ni}(\text{CO})_4$ (Figure 2.2 (a)) is the first Ni^0 compound that was used by Mond et al to produce Ni film in 1885.^{5b} It is considered as the first precursor for CVD in industrial application and still being used to date. Although the liquid $\text{Ni}(\text{CO})_4$ provides pure Ni film at low temperature. However, the highly toxicity has limited this compound from application. In 2003, Choi et al reported a series of tetrakis(trialkyl phosphine)nickel complexes as new Ni^0 precursors. These complexes are quite volatile and exhibit high thermal stability. The complex $\text{Ni}[\text{P}(\text{OEt})_3]_4$ (Figure 2.2 (b)) can deposit highly pur Ni film (> 99 %) at 200 °C using Ar as carrier gas.^{5a} Another Ni^0 precursor is tetrakis(trifluorophosphane) nickel compound $\text{Ni}(\text{PF}_3)_4$ (Figure 2.2 (c)). Ogura et al reported a new route to synthesize the compound from

nickelocene and PF_3 in high yield for CVD application. This liquid precursor has a vapor pressure of 215 Torr at 30 °C. It can deposit pure Ni film (99 %) at low temperature (200 °C) using He as carrier gas.^{5d} This compound is less toxic than $\text{Ni}(\text{CO})_4$ but the decomposed product (PF_3 ligand) has high toxicity.

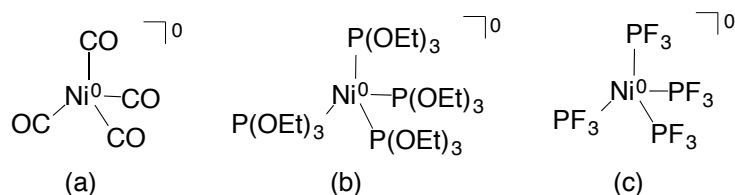
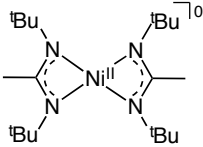
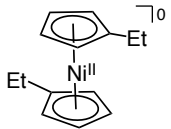
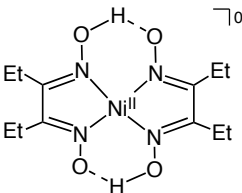
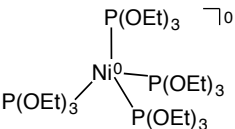
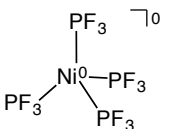
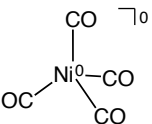


Figure 2.2 Zero-valent nickel (Ni^0) compounds have been utilized as MOCVD precursor to deposit Ni thin film

The most common Ni^{II} MOCVD precursors are nickelocene $\text{Ni}((\eta^5\text{-C}_5\text{H}_5))$ and its derivatives.^{6b} These precursors are less toxic but also less volatile than $\text{Ni}(\text{CO})_4$. The purity of Ni film deposited from nickelocene derivatives can be optimized by deposition conditions. However, due to strong interaction between Ni and ligands, these precursors suffer from unavoidable contamination of C from ligands even at optimized conditions using H_2 as reducing gas.

For application the highly pure Ni thin film is demanded. Many researches have been conducted to develop new precursor for this aim. However, only few Ni MOCVD precursors are able to deposit Ni film with high purity. Table 2.1 lists the Ni precursors that can deposit Ni film with low contamination (< 2%).

Table 2.1: The Ni precursors have been used to prepare pure Ni films with contamination < 2 % by MOCVD

Ni precursors	Reducing or carrier gas	Contamination (%)	Vapor pressure (Pa)	Deposition temperature (°C)	Ref.
	H ₂ or/and NH ₃	0	6.7 (at 95 °C)	200	4a
	H ₂	1.3–2.0	50 (at 73 °C)	250	4b
	H ₂	< 2	3000 (at 200 °C)	350	6a
	Ar	0	6.7 (at 96 °C)	200	5a
	He	< 1	28700 (at 30 °C)	180	5d
	He	0	53000 (at 26 °C)	100	5b

The previously reported Ni^0 and Ni^{II} MOCVD precursors suffer from problems with their carrier or/and reactive gas requirements.

In order to deposit highly pure Ni film, the Ni^{II} MOCVD precursors need hydrogen (H_2) as a reactive or reducing gas that reduces Ni^{II} to Ni^0 (metallic Ni) and then eliminates impurities from the growing Ni film. Without H_2 gas, the deposition is governed by the thermolysis requiring high deposition temperature. Which not only consumes much energy but also causes the decomposition of compound's ligand resulting high contamination on deposited film. However, using H_2 limits the conformity of the film deposited on high-aspect-ratio substrate because of the rapid recombination of H_2 atoms on the walls of the trenches. Moreover, H_2 gas is neither cheap nor safe, employing H_2 in such heating system as MOCVD increases the risk of explosion.

On the other hand, the Ni^0 compounds essentially do not required reactive gas to form Ni film because of their intrinsic metal. Only inert gas is needed as the carrier gas that transports vapor-phase precursor to heated substrate to form the film. In this case, precursor chemistry is demanded. The precursor should be thermally stable enough to vaporize without decomposition but it should be decomposed at low temperature enough to release ligands clearly before film formation. The previously reported Ni^0 MOCVD precursors routinely use Ar or He as the carrier gases.⁵ However, these are scarce and expensive. A safe, cheap and abundant gas such as N_2 is desirable. This requirement motivates the author to synthesize a novel Ni^0 complex that is able to deposit pure Ni film at low temperature using N_2 as carrier gas.

2.1.3. Strategy to resolve the obstacles

As mentioned in the previous section, the Ni^0 compounds are preferable to Ni^{II} compounds because they do not require the reactive gas to deposit high purity Ni film

at low temperature. However, known Ni^0 precursors suffer from drawback of using Ar or He. To overcome this obstacle, a new Ni^0 compound should be designed and synthesized.

Bis(1,5-cyclooctadiene)nickel $\text{Ni}^0(\text{COD})_2$ is a well-known zero-valent complex. It has been used as catalyst and the starting material to synthesize other Ni compounds. However, this complex has never been utilized as a MOCVD precursor due to its non-volatile and thermally unstable property.

To serve as a MOCVD precursor, a complex should be high volatility and reasonable thermal stability. Recently, 1,2-bis(trimethylsilyl)acetylene (**L**) has been used as a ligand to synthesize zero-valent cobalt complex for MOCVD application.^{8a} Furthermore, the silyl ligands have been demonstrated to thermally stabilize organometallic complex. Several silyl-substituted complexes have been applied successfully as MOCVD precursor.^{8b}

With these in mind, the author attempts to substitute one COD ligand of $\text{Ni}^0(\text{COD})_2$ by the ligand **L** to afford a novel Ni^0 complex **1** (Figure 2.3). The ligand **L** is expected to thermally stabilize complex **1** and the steric silyl group may assist the volatility of this complex.

The molecular design of complex **1** is expected to provide a good Ni MOCVD precursor for deposition of highly pure Ni film using cheap and safe gas N_2 as the carrier gas.

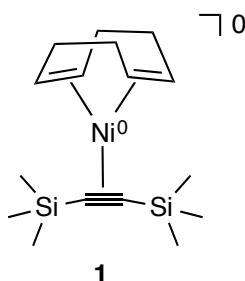


Figure 2.3 Chemical structure of Ni^0 complex **1**

2.2. RESULTS AND DISSCUSSION

2.2.1. Synthesis and characterization of a novel Ni⁰ complex

The Ni⁰ precursor, [Ni⁰(COD)(L)] {**1**, COD = 1,5-cyclooctadiene, L = 1,2-bis(trimethylsilyl)acetylene}, was synthesized conveniently in high yield from commercial available reagents. The complex **1** (yield 83 %) was obtained from the reaction of bis(cyclooctadiene)nickel (Ni⁰(COD)₂) with an excess amount of the acetylene derivative ligand L (1,2-bis(trimethylsilyl)acetylene) in dry tetrahydrofuran (THF) at low temperature under an N₂ atmosphere (Figure 2.4). The air and moisture sensitive compound **1** was characterized by ¹H NMR (Figure 2.5), ¹³C{¹H} NMR (Figure 2.6) spectroscopies, elemental analysis and X-ray analysis (Figure 2.7).

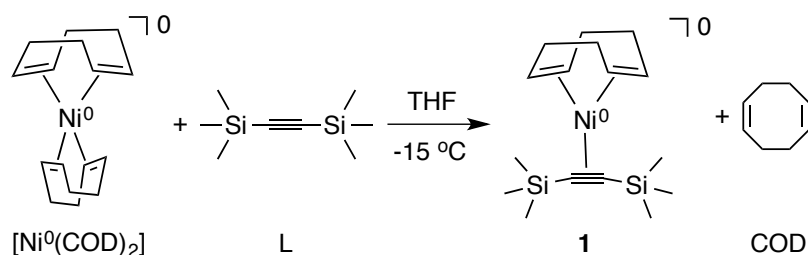


Figure 2.4 Synthesis of complex **1** from the reaction of $[\text{Ni}^0(\text{COD})_2]$ with ligand **L**, 1,2-bis(trimethylsilyl)acetylene.

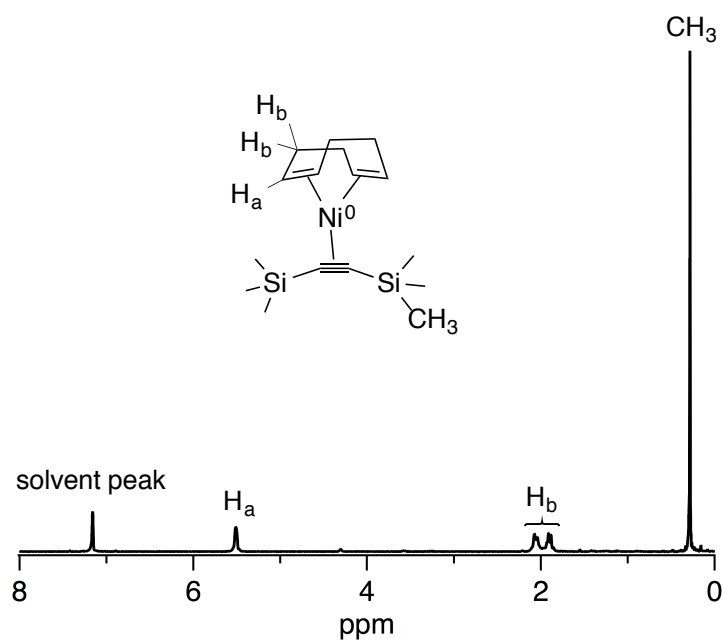


Figure 2.5 ^1H NMR spectrum of complex **1** in C_6D_6 at room temperature.

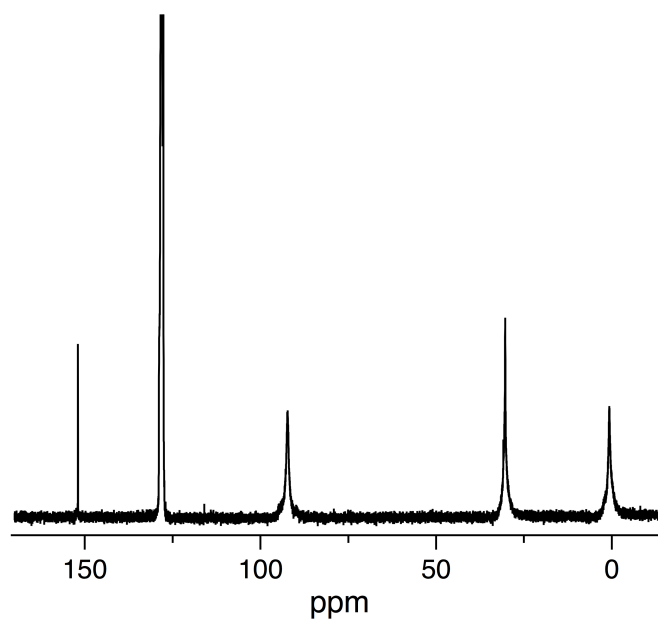


Figure 2.6 $^{13}\text{C}\{^1\text{H}\}$ NMR spectrum of complex **1** in C_6D_6 at room temperature.

Complex **1** was recrystallized from its concentrated hexane solution at $-80\text{ }^{\circ}\text{C}$ overnight to afford yellow crystals that is suitable for X-ray crystallography. Figure 2.7 shows the ORTEP drawing of complex **1**, in which the Ni atom is coordinated to the C \equiv C bond of the acetylene unit of L in an η^2 -fashion and the C=C bonds of the COD ligand in an η^4 -fashion. The distance of C1–C2 {1.276(2) Å} is similar to that of a free acetylene molecule (1.20 Å)⁹ and the bond-lengths of C11–C12 {1.368(3) Å} and C15–C16 {1.373(3) Å} are comparable to that of a free ethylene molecule (1.34 Å).¹⁰ The C \equiv C bond distance {1.276(2) Å} of complex **1** is within the range of 1.251(9)–1.284(5) Å found for the Ni⁰ compounds having COD and acetylene derivatives.¹³ The Si–C–C bonds deviate from linear {Si1–C1–C2 = 150.23(14) $^{\circ}$ and Si2–C2–C1 = 151.65(14) $^{\circ}$ } probably due to steric repulsion of the Si(CH₃)₃ groups against the COD ligand.

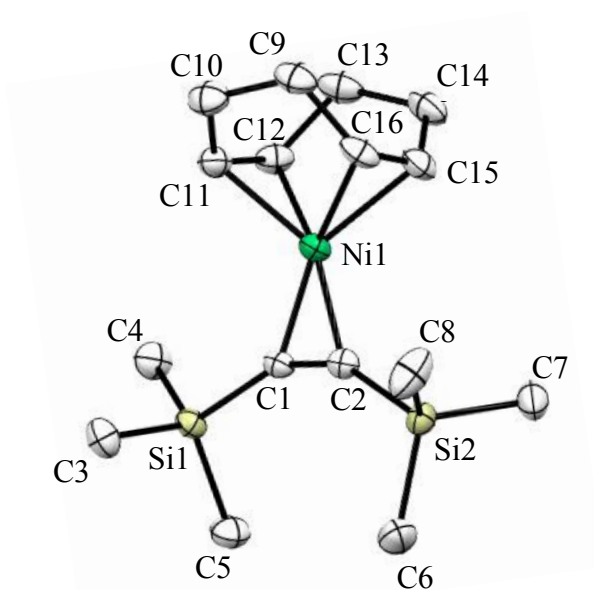


Figure 2.7 An ORTEP drawing of complex **1** with thermal ellipsoids at the 50% probability level, the hydrogen atoms are omitted for clarity.

Table 2.2: Selected interatomic distances ($l/\text{\AA}$) and angles ($\phi/^\circ$) for complex **1**

Ni1–C1	1.9108(16)	Ni1–C2	1.9121(17)
Ni1–C11	2.0815(18)	Ni1–C12	2.0925(18)
Ni1–C15	2.0896(19)	Ni1–C16	2.1001(18)
C1–C2	1.276(2)	C9–C10	1.543(3)
C10–C11	1.511(3)	C11–C12	1.368(3)
C12–C13	1.517(3)	C13–C14	1.539(3)
C14–C15	1.505(3)	C15–C16	1.373(3)
C9–C16	1.509(3)	C1–Si1	1.8506(16)
C2–Si2	1.8412(17)	C1–Ni1–C2	38.99(7)
C11–Ni1–C12	38.26(7)	C15–Ni1–C16	38.25(7)
Si1–C1–C2	150.23(14)	Si2–C2–C1	151.65(14)

Table 2.3: Crystallographic data for complex **1**

Formula	C ₁₆ H ₃₀ NiSi ₂
<i>F</i> _w	337.28
Crystal system	monoclinic
Space group	P2 ₁ /c (#14)
<i>a</i> (Å)	15.502(3)
<i>b</i> (Å)	10.138
<i>c</i> (Å)	11.757
α (deg)	90
β (deg)	90.551(3)
γ (deg)	90
<i>V</i> (Å ³)	1847.8(7)
<i>Z</i>	4
μ (cm ⁻¹)	11.67
<i>F</i> (000)	728.0
<i>D</i> _{calcd} (g/cm ³)	1.212
Temperature (K)	93
Reflections collected	3630
Independent reflection	4185
<i>R</i> ₁ [<i>I</i> > 2 σ (<i>I</i>)]	0.0318
<i>wR</i> ₂ (all data)	0.0892
Goodness-of-fit	1.036

2.2.2. Physical properties of complex 1

The sufficient volatility is a critical requirement for a MOCVD precursor. Complex **1** was tested for volatility in a sublimation apparatus under vacuum giving a vapor pressure of 90.7 Pa at 45 °C. This is one of the highest values for the known Ni^{II} and Ni⁰ precursors (Table 2.1).⁴⁻⁸

Thermalgravimetry-differential thermal analysis (TG-DTA) is a powerful tool to estimate the physical properties of a compound such as, melting point, vaporization and thermal stability, which are very useful to know before carrying out a MOCVD experiment. In order to ensure that complex **1** is suitable for MOCVD, the thermal properties were determined by TG-DTA. The measurement was obtained at a linear heating rate of 10 °C min⁻¹ under a N₂ flow rate of 100 standard cc min⁻¹ (sccm) (Figure 2.8)

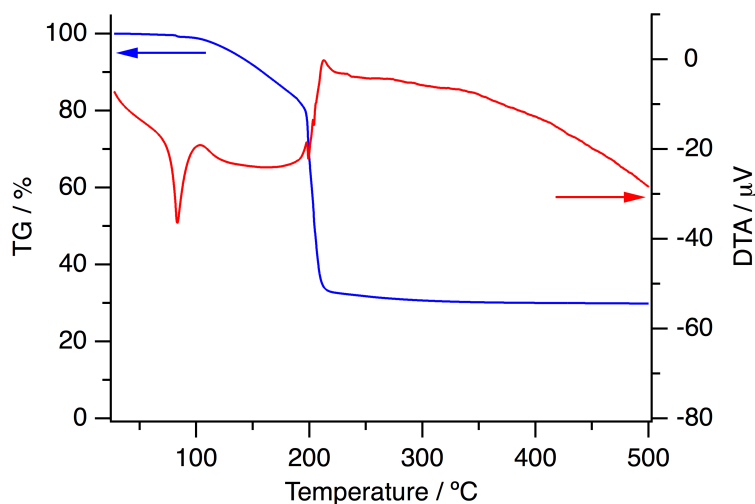


Figure 2.8 TG-DTA of **1** (heating rate: 10 °C min⁻¹ flow rate of N₂ gas: 100 sccm).

The TG curve shows that the weight loss begins around 110 °C and ends at about 200 °C accompanying with an endothermic at DTA plot. These data revealed that complex **1** sublimes at about 110 °C and likely decomposes at 200 °C. The DTA plot

shows an endothermic peak at 83 °C without weight loss in the TG curve suggesting of a melting without decomposition.

Based on the thermal properties that were determined above, the complex **1** is suitable as a MOCVD precursor.

2.2.3. Deposition and characterization of Ni film

Ni films were deposited from complex **1** on a SiO₂ substrate at various temperatures using a tube-type CVD apparatus under a flow of N₂ as carrier gas. The pressure of CVD reactor was controlled to 75 Pa and N₂ gas flow rate was set at 10 sccm. The temperature of precursor **1** was fixed at 55-60 °C and the substrate temperature was varied in the range of 190-250 °C. The substrate temperature was optimized at 200 °C, at which the deposited Ni film showed the best performance. The deposited film appeared silvery lustrous metal.

Annealing is usually used after deposition process to improve the morphology and/or to reduce the contamination of post-deposition film. In this work, the deposited Ni film was annealed at 300 °C under a flow of N₂ gas for 1 h before characterization.

After annealing was completed, the deposited Ni film was characterized by scanning electron microscopy (SEM), Atomic force microscopy (AFM), X-ray photoelectron spectroscopy (XPS) and X-ray diffraction (XRD).

The physical properties of Ni film such as conductivity strongly depend on its purity. For MOCVD process, the precursor is a metal-organic or organometallic compounds so the contaminants are usually carbon (C) some elements originating from the compound's ligand.

In order to investigate the purity and composition of the deposited Ni film, an XPS measurement was employed. The adventitious C usually contaminates the surface of deposited Ni film after exposure to air. The surface can even be oxidized by

O₂ in air. Therefore, an Ar ions beam was used inside XPS measurement chamber to etch the surface of Ni film before collecting data. Figure 2.9 shows the XPS result of a Ni film after being etched by sputtering with an Ar ions beam. Only the peaks derived from Ni were observed. There was no peak of C, O or Si (Figure 2.9 (A)) suggesting the high purity of Ni film. The contamination was estimated by XPS with a significant low value (< 1%). The binding energies of Ni 2p_{1/2} and Ni3p_{3/2} were 870.2 eV and 852.7 eV (Figure 2.9 (B)) respectively, corresponding to those found for metallic Ni (Ni⁰).^{13,14} These results demonstrate that complex **1** is an excellent MOCVD precursor that is able to deposit high purity Ni film using N₂ as carrier gas without adding any reactive gas.

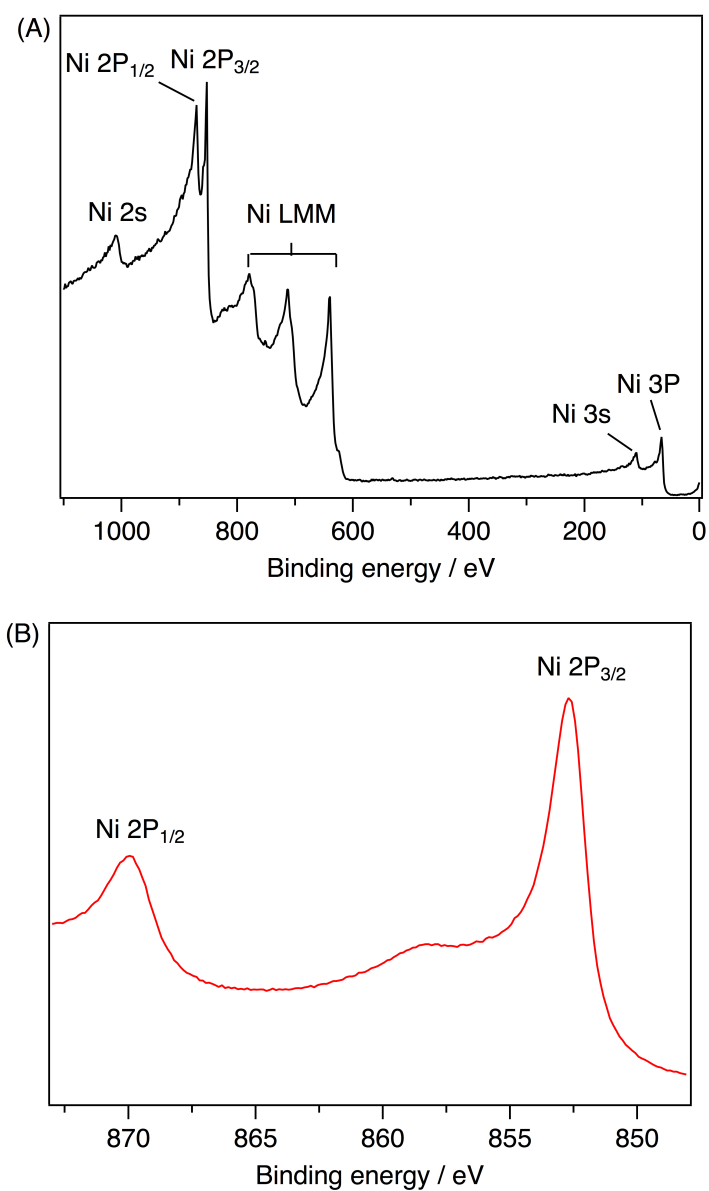


Figure 2.9 (A) XPS result of a Ni thin film growth from complex **1** at 200 °C under flowing of N₂ gas, (B) narrow-scanned of Ni 2p region

The morphology of the Ni films was observed by scanning electron microscopy (SEM) and atomic force microscopy (AFM).

The SEM images of a Ni film deposited on SiO₂ substrate are shown in Figure 2.10. The surface view reveals variable-sized, multiform crystalline grains. A thickness of 150 nm was estimated by the cross-sectional view of Ni thin film. The Ni film exhibits almost planar, continuous and uniform thickness.

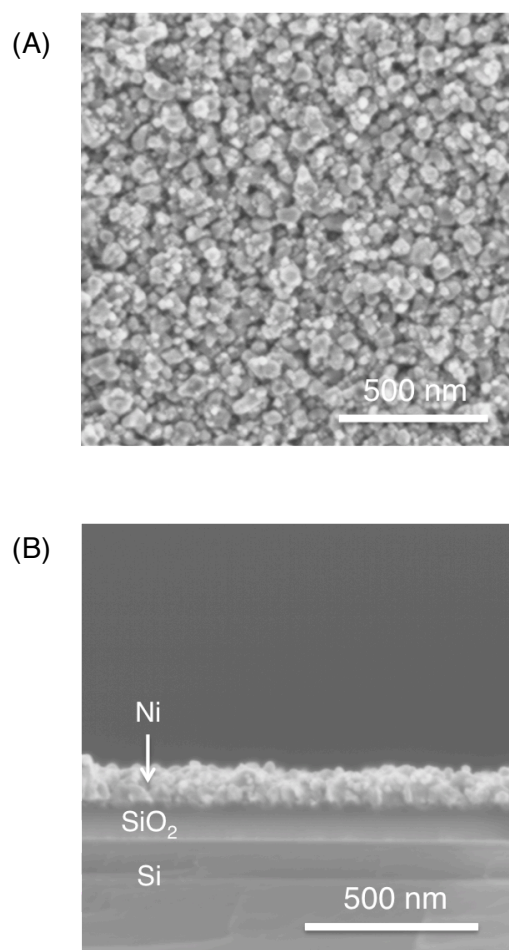


Figure 2.10 SEM images of a Ni film deposited from **1** at 200 °C under a flow of N₂ gas. (A) Surface – and (B) cross-sectional views.

In order to investigate the surface roughness of the deposited Ni film, AFM images were obtained. Figure 2.11 shows AFM images of a Ni film deposited from **1** at 200 °C that illustrates a quite smooth and dense film. The root-mean-square (RMS) roughness value was determined as 11.3 nm for a deposited Ni film with the thickness of 150 nm ($\approx 7.5\%$).

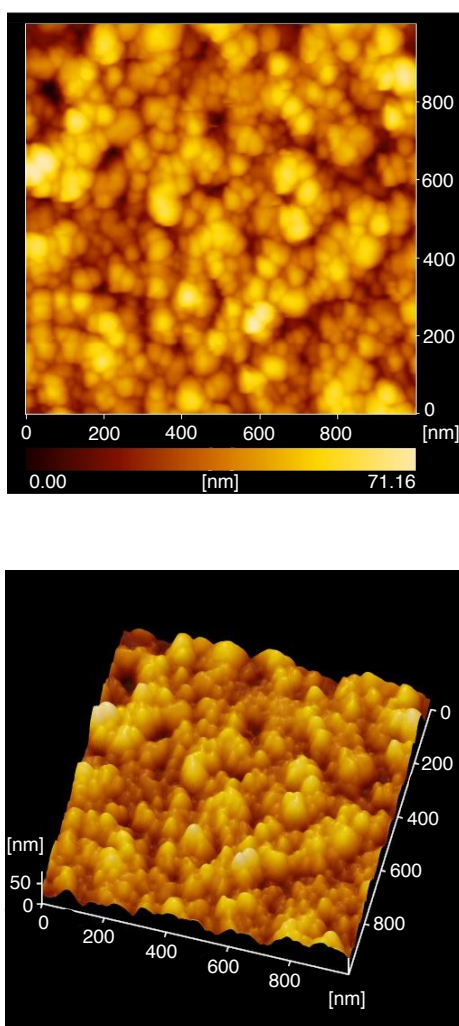


Figure 2.11 AFM images of a Ni film deposited from **1** at 200 °C under a flow of N₂ gas. (a) two – and (b) three – dimensional views.

XRD measurement was performed to study the structure of the deposited Ni film. The XRD pattern is presented in Figure 2.12. A sharp diffraction peak at $2\theta = 44.3^\circ$ and another peak at $2\theta = 52^\circ$ were observed. These peaks belong to face-centered-cubic-Ni (fcc-Ni) (111) and (200) face, respectively.

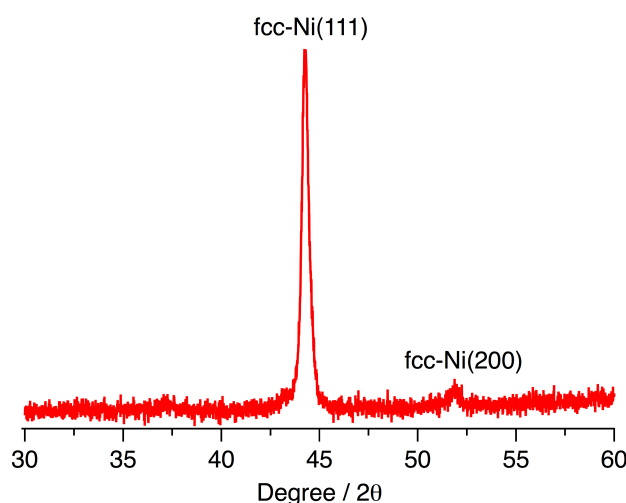


Figure 2.12 An XRD spectrum of a Ni film deposited from **1** at 200 °C under a flow of N₂ gas. (fcc = face centered cubic).

Highly conductive Ni film is desirable especially for application in electrical and electronic devices. The resistivity measurement was carried out by a four-point probe method. A value of 43 $\mu\Omega$ cm was determined for a 150 nm thick film deposited from **1**. This value is relatively low, which is lower than the previously reported value for Ni thin film (70 $\mu\Omega$ cm)^{4f} and higher than pure bulk Ni (6 $\mu\Omega$ cm).^{5a} The high purity may result in the high conductivity of the Ni film. The density of the deposited film also influences its resistivity. Multi-size crystal grains may lead to higher density than the previously uniform grain. However, the granular structure renders a low density of the Ni film comparing to bulk Ni.

2.3. CONCLUSIONS

In conclusion, a novel zero-valent Ni complex **1** was prepared conveniently in high yield from commercial-available reagents. The complex was fully characterized by ^1H , $^{13}\text{C}\{^1\text{H}\}$ NMR, elemental analysis and X-ray crystallography whose results agree with the proposed structure. The vapor pressure of **1** was determined as one of the highest values for the known Ni^{II} and Ni^0 MOCVD precursors. The thermal property measurement results showed that complex **1** is a good precursor for MOCVD. The Ni film was obtained by MOCVD of **1** at low temperature deposition using a cheap and safe N_2 gas as the carrier gas. The XPS results revealed a highly pure Ni film without contamination. A fairly smooth Ni film was determined by AFM with low root-mean-square roughness. This complex is the first example of a Ni precursor that is able to deposit highly pure Ni film using N_2 as the carries gas without addition of any reducing gas. The author believes this novel Ni organometallic compound will be a good candidate for MOCVD application.

2.4. EXPERIMENTAL

2.4.1. Materials and methods

All manipulations were carried out under an N₂ gas using either standard Schlenk or glovebox techniques. Tetrahydrofuran (THF) as distilled Na/benzophenone under an N₂ atmosphere. Hexane and methanol were distilled under an N₂ gas over CaH₂ and Mg/I₂ respectively. Bis(cyclooctadiene)nickel Ni⁰(COD)₂; COD = 1,5-cyclooctadiene) and 1,2-bis(trimethylsilyl)acetylene were purchased from Sigma Aldrich and used without further purification.

¹H and ¹³C{¹H} NMR spectra were recorded on a JEOL JNM-AL300 at 25 °C. The chemical shifts were referenced to benzene (¹H NMR: δ 7.16 and ¹³C{¹H} NMR: δ 128.06 ppm respectively).¹ An elemental analysis data was obtained by using a PerkinElmer 2400II series CHNS/O analyzer using Ar as the carrier gas.

Ni⁰ film was analyzed by scanning electron microscopy (SEM) using a Hitachi SU8000. The thickness of Ni⁰ film was determined by a cross-sectional SEM image. In order to observe the surface morphology and estimate the root mean square (RMS) roughness value, atomic force microscopy (AFM) was carried out using a Nanocute (Hitachi High-Tech Science Corporation). The composition and purity of the deposited film were investigated by X-ray photoelectron spectroscopy (XPS) using an ULVAC PHI 5000 VersaProbe II system with an Al anode X-ray source. Binding energies were calibrated by the Si 2p peak of SiO₂ substrates at 103.3 eV.² The crystal orientation of the deposited Ni⁰ film was evaluated by X-ray diffraction (XRD) patterns using an X-ray diffractometer (Rigaku Ultramax IV) with Cu-Kα radiation generated at 40 kV and 30 mA {scan speed: 0.02° min⁻¹ (2θ = 30–60°)}. The electrical resistivity of Ni film was determined by a four-point probe method at 25 °C using a Loresta EP MCP-T360 (Mitsubishi).

2.4.2. Synthesis of complex **1**

Synthesis of **1**

0.30 ml (1.39 mmol) of 1,2-bis(trimethylsilyl)acetylene (**L**) was added to 100 mg (0.36 mmol) of $\text{Ni}^0(\text{COD})_2$ in 5 ml of THF at $-78\text{ }^\circ\text{C}$. The resulting solution was stirred for 12 h at $-15\text{ }^\circ\text{C}$, then the solvent was evaporated in vacuo while the solution was kept at $-10\text{ }^\circ\text{C}$. The residue was dissolved in 3.0 ml of cold methanol, filtration to remove insoluble compound(s). The filtrate was allowed to stand overnight at $-35\text{ }^\circ\text{C}$ to afford yellow crystals. The product was filtered and dried under vacuum (yield 83 % based on $\text{Ni}^0(\text{COD})_2$). The complex **1** is sensitive to air and moisture. However, it can be stored indefinitely at $0\text{ }^\circ\text{C}$ in an N_2 atmosphere.

^1NMR (300 MHz, in C_6D_6): δ 5.51 (t, 4H, C_8H_{12}), 2.05 (m, 4H, C_8H_{12}), 1.90 (m, 4H, C_8H_{12}), 0.29 (s, 18H, $\text{Si}(\text{CH}_3)_3$). $^{13}\text{C}\{^1\text{H}\}$ NMR (75 MHz, in C_6D_6): δ 152.0, 92.3, 30.4, 0.7. Anal. Calcd for **1**: $\text{C}_{16}\text{H}_{30}\text{NiSi}_2$: C, 56.98; H, 8.97. Found: C, 57.03; H, 9.05.

X-ray crystallographic analysis of **1**

The yellow crystal of **1** that is suitable for X-ray crystallography was recrystallized from its concentrated hexane solution at $-80\text{ }^\circ\text{C}$ overnight. The measurement was conducted on a Rigaku/MSK Saturn CCD diffractometer with confocal monochromated Mo-K radiation ($\lambda = 0.7107\text{ \AA}$). Data was collected and processed using the CrystalClear program. All calculations were performed using the CrystalStructure crystallographic software package except for refinement, which was performed using SHELXL-97. Crystallographic data for **1** has been deposited with the Cambridge Crystallographic Data Centre as Supplementary Publication No. CCDC-1045076. Copies of the data can be obtained free of charge on application to CCDC,

12 Union Road, Cambridge CB2 1EZ, UK (fax: +44-1223-336-033; e-mail: deposit@ccdc.cam.ac.uk).

Thermal properties of **1**

A thermogravimetry–differential thermal analysis (TG–DTA) was carried out to investigate thermal properties of **1** using an EXSTAR TG-DTA7300 instrument. In a glovebox, 15 mg of **1** was loaded in a sealed-type aluminum crucible. In order to prevent exposure of **1** to air, the crucible lid was poked with a pin to make an exhaust hole just before the measurement. The measurement was made under N₂ gas with flow rate of 100 standard cc min⁻¹ (sccm) at a linear heating rate of 10 °C min⁻¹ under atmospheric pressure.

2.4.3. Deposition of the Ni film from complex **1**

Ni film was deposited onto a SiO₂ substrate (80 nm layer of native SiO₂ on Si) using a tube type chemical vapor deposition (CVD) reactor with glass tube diameter of 2.6 cm. A distance of 4.5 cm between SiO₂ substrate and precursor **1** was fixed. Precursor **1** was heated to vaporization at 55-60 °C under a pressure of 75 Pa using N₂ as carrier gas (flow rate: 10 sccm), while the SiO₂ substrate was maintained at 200 °C. The deposited Ni film was then treated by annealing at 300 °C for 1 h under N₂ gas (flow rate: 10 sccm). The Ni film was characterized by X-ray photoelectron spectroscopy (XPS), scanning electron microscopy (SEM), atomic force microscopy (AFM) and X-ray diffraction (XRD).

REFERENCES

1. J. F. Rohan, G. O’Riordan and J. Boardman, *Appl. Surf. Sci.*, 2002, **185**, 289–297.
2. (a) M. J. Kenney, M. Gong, Y. Li, J. Z. Wu, J. Feng, M. Lanza and H. Dai, *Science*, 2013, **342**, 836–840; (b) P. A. Premkumar, A. Dasgupta, P. Kuppusami, P. Parameswaran, C. Mallika, K. S. Nagaraja and V. S. Raghathan, *Chem. Vap. Deposition*, 2006, **12**, 39–45.
3. E. E. Shalygina, L. V. Kozlovski, N. M. Abrosimova and M. A. Mukasheva, *Phys. Solid State*, 2005, **47**, 684–689.
4. (a) Z. Li, R. G. Gordon, V. Pallem, H. Li and D. V. Shenai, *Chem. Mater.*, 2010, **22**, 3060–3066; (b) S. E. Alexandrov and V. S. Protopopova, *J. Nanosci. Nanotechnol.*, 2011, **11**, 8259–8263; (c) S. I. Dorovskikh, A. V. Alexeyev, N. V. Kuratieva, T. V. Basova, V. G. Kiselev, L. A. Sheludyakova, Y. V. Shubin, N. B. Morozova and I. K. Igumenov, *J. Organomet. Chem.*, 2013, **741–742**, 122–130; (d) G. I. Zharkova, S. I. Dorovskikh, S. V. Sysoev, I. P. Asanov, A. V. Panin, N. B. Morozova and I. K. Igumenov, *Surf. Coat. Technol.*, 2013, **230**, 290–296; (e) S. I. Dorovskikh, E. A. Bykova, N. V. Kuratieva, L. N. Zelenina, Y. V. Ahubin, N. B. Morozova and I. K. Igumenov, *J. Organomet. Chem.*, 2012, **698**, 22–27; (f) T. Kada, M. Ishikawa, H. Machida, A. Ogura, Y. Ohshita and K. Soai, *J. Cryst. Growth*, 2005, **275**, e1115–e1119; (g) V. V. Bakovets, V. N. Mitkin and N. V. Gelfond, *Chem. Vap. Deposition*, 2005, **11**, 368–374; (h) M. Ishikawa, T. Kada, H. Machida, Y. Ohshita and A. Ogura, *Jpn. J. Appl. Phys.*, 2004, **43**, 1833–1836; (i) L. Brissonneau, D. de Caro, D. Boursier, R. Madar and C. Vahlas, *Chem. Vap. Deposition*, 1999, **5**, 143–149; (j) T. Maruyama and T. Tago, *J. Mater. Sci.*, 1993, **28**, 5345–5348; (k) R. L. Van Hemert, L. B. Spendlove and R. E. Sievers, *J. Electrochem. Soc.*, 1965, **112**, 1123–1126.

5. (a) H. Choi, S. Park and T. H. Kim, *Chem. Mater.*, 2003, **15**, 3735–3738; (b) L. Mond, C. Langer and F. Quincke, *J. Chem. Soc., Trans.*, 1890, **57**, 749–753; (c) F. Fau-Canillac and F. Maury, *Surf. Coat. Tech.*, 1994, **64**, 21–27; (d) Y. Ohshita, M. Ishikawa, T. Kada, H. Machida and A. Ogura, *Jpn. J. Appl. Phys.*, 2005, **44**, L315–L317.
6. (a) J. D. Martin, P. Hogan, K. A. Abboud and K.-H. Dahmen, *Chem. Mater.*, 1998, **10**, 2525–2532; (b) V. S. Protopopova and S. E. Alexandrov, *Surf. Coat. Tech.*, 2003, **230**, 316–321
7. M. Basato, E. Faggin, C. Tubaro and A. C. Veronese, *Polyhedron*, 2009, **28**, 1229–1234.
8. (a) C. Georgi, A. Hildebrandt, T. Waechtler, S. E. Schulz, T. Gessner and H. Lang, *J. Mater. Chem. C.*, 2014, **2**, 4676–4682; (b) A. Tuchscherer, C. Georgi, N. Roth, D. Schaarschmidt, T. Ruffer, T. Waechtler, S. E. Schulz, S. Oswald, T. Gessner and H. Lang, *Eur. J. Inorg. Chem.*, 2012, **30**, 4867–4876.
9. J. McMurry, *Fundamentals of Organic Chemistry, International Edition 7th Ed*, Cengage Learning, 2011.
10. (a) D. Walther, T. Klettke, H. Görls and W. Imhof, *J. Organomet. Chem.*, 1997, **534**, 129–137; (b) D. Walther, T. Klettke, A. Schmidt, H. Görls and W. Imhof, *Organometallics*, 1996, **15**, 2314–2319; (c) D. Walther, A. Schmidt, T. Klettke, W. Imhof and H. Görls, *Angew. Chem. Int. Ed.*, 1994, **33**, 1373–1376; (d) R. Goddard, B. Apotecher and H. Hoberg, *Acta Cryst.*, 1987, **C43**, 1290–1293.
11. J. F. Moulder, W. F. Stickle, P. E. Sobol and K. D. Bomben, *Handbook of X-ray Photoelectron Spectroscopy*, Physical Electronics, Inc., Minnesota, 1995.
12. M. C. Biesinger, B. P. Payne, A. P. Grosvenor, L. W. M. Lau, A. R. Gerson and R. St. C. Smart, *Appl. Surf. Sci.*, 2011, **257**, 2717–2730.

CHAPTER 3

AN IRIIDIUM-SILICON OXIDE FILM AS A HIGHLY ACTIVE WATER-OXIDATION CATALYST IN ACIDIC MEDIA

ABSTRACT

In this work, an amorphous Si oxide-doped Ir oxide film (IrSi oxide film) was prepared by MOCVD using an iridium-silyl (Ir-Si) complex, $[\text{Ir}^{\text{V}}(\text{C}_5\text{Me}_5)(\text{H})_2(\text{SiEt}_3)_2]$ (**2**) as a single precursor and successive electrochemical oxidization (Figure 3.1). The film was characterized by several methods such as: X-ray photoelectron spectroscopy (XPS), scanning transmission electron microscopy (STEM) equipped energy dispersive X-ray spectroscopy (EDS) mappings, scanning electron microscopy (SEM) and X-ray diffraction (XRD) spectroscopy. Those determined an amorphous structure of IrSi oxide film with homogeneously distribution of Ir and Si elements in the solid phase. The IrSi oxide deposited onto fluorine doped tin oxide (FTO) substrate exhibits high catalytic activity and stability for water-oxidation catalyst in acidic media. The turnover frequency (TOF) of

electrochemical water-oxidation by this film is higher than any previously reported Si oxide-doped Ir oxide materials and even higher than Ir oxide in acidic condition. This is the first example of successful enhancement of catalytic ability and stability as well as decrement of the scarce and expensive Ir content by doping of an abundant and cheap Si oxide.

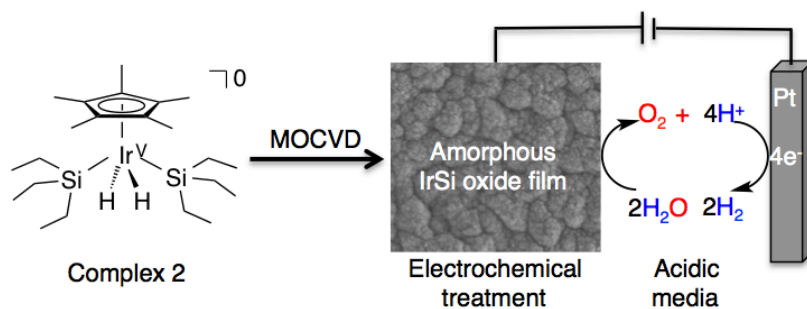


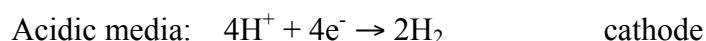
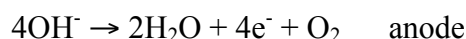
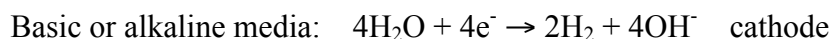
Figure 3.1 The Iridium-Silyl complex, $[\text{Ir}^{\text{V}}(\eta^5\text{-C}_5\text{Me}_5)(\text{H})_2(\text{SiEt}_3)_2]$ (**2**) used as a single MOCVD precursor to prepare amorphous IrSi oxide film as a highly active and stable water-oxidation catalyst in acidic regime.

3.1. INTRODUCTION

3.1.1. Electrochemical water-oxidation catalyst

Hydrogen is considered as the best energy carrier that provides reliable and affordable clean energy.¹ Currently, hydrogen is mainly produced by steam reformation of hydrocarbons.^{1d} However, this process consumes much energy for heating and it utilizes the non-renewable fossil fuel source. Electrocatalytic splitting of water is expected to be the most attractive approaches because hydrogen can be generated from water and electricity obtaining from renewable sources such as sunlight and wind-turbine.^{1e}

Electrocatalytic water splitting or water electrolysis reaction can be divided into two half-redox reactions: Oxygen evolution reaction (OER) taking place at anode and hydrogen evolution reaction (HER) occurring at cathode. Depending upon the basic electrolyte (alkaline) or acidic electrolyte being used, these two half-redox reactions can be describe by the following equations:



Basic or alkaline water electrolysis is a system that contains two electrodes working in a liquid alkaline electrolyte solution. In this system, anode and cathode are separated by a diaphragm which keeps the product gasses from one another and allows only the hydroxide ions and water molecules to transport between two electrodes (Figure 3.2 (A)).

Acidic water electrolysis relates to polymer electrolyte membrane (PEM) electrolysis. In this system, anode and cathode are equipped into two different sides of a solid polymer electrolyte (SPE), which separates product gases, allows protons and inhibits electron to transfer from one electrode to the other (Figure 3.2 (B)).

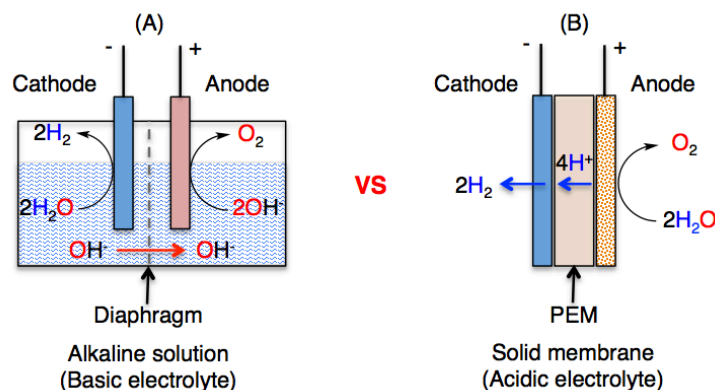


Figure 3.2 Diagram of an alkaline electrolysis and a polymer electrolyte membrane (PEM) electrolysis.

Compared with alkaline water electrolysis, polymer electrolyte membrane (PEM) water electrolysis offers many advantages such as higher operational current density and higher energy efficiency. In case of alkaline water electrolysis, the diaphragm cannot prevent a small amount of product gas diffusion causing the recombination of oxygen and hydrogen, which will be catalyzed to reproduce water. This will reduce the efficiency and the purity of product gas as well as the safety of the process. In contract, PEM water electrolysis can overcome the issues of alkaline water electrolysis such as partial load, low current density and low-pressure operations. For application in industrial devices, the acidic polymer electrolyte membrane (PEM) water electrolysis is of choice due to its advantages.

Although acidic water electrolysis has many advantages over its counterpart (alkaline water electrolysis), this system remained a big problem. The oxidation step happening at anode is a challenging because it requires the elimination of 4 electrons

and 4 protons to form O - O bond. Furthermore, the reaction is held in acidic regime, it requires corrosion stability. Because of the above-mentioned reasons, only noble metal oxides such as Ir oxides and Ru oxides can be used as anode for acidic water electrolysis. The Ru oxides sometimes exhibit higher catalytic ability than Ir oxides, but they are less stable than Ir oxide in acidic condition.

3.2.2. Previous work and obstacles

As mentioned previously, Ir oxides are the best catalyst for water-oxidation in acidic media, in terms of high catalytic activity and long-term stability. However, Ir is very expensive and scarce, which hinders Ir from its practical application. Many research efforts have been made to reduce the amount of Ir loading in the anode and improve the catalytic activity. Two approaches have been used for decreasing the Ir content: 1) Developing new preparation methods that provide novel morphologies and structures with high active area. 2) Doping the other abundant components into Ir oxides.

The new preparation methods have been discovered and applied to increase the catalytic ability and stability. It has demonstrated that the catalytic activity and stability of Ir oxides strongly depend upon the preparation methods offering novel morphologies and surface structures. There have been several methods for the preparation of Ir oxides for example, the thermal decomposition of Ir salts produces active Ir oxide on the electrode. Active Ir oxide nanoparticles can also be formed in solution by the hydrolysis of Ir precursors.^{4d} Meanwhile, amorphous Ir oxide films with high catalytic activity for water oxidation have been formed by electrochemical deposition using an organometallic Ir complex.^{4e} Recently, the irradiation of an organometallic Ir complex by UV-light followed by heating also affords an amorphous Ir oxide film.^{4c} The sputtering and atomic layer deposition (ALD) are the other methods for depositing Ir oxide films. Each of the above methods has its

characteristic advantages. However, they all suffer from the same drawbacks. The wet solution chemical methods such as thermal decomposition and hydrolysis cannot deposit catalysts on anode directly but require many steps for fabrication electrode. Additionally, the films formed by these methods often have poor attachment. On the other hand, the gas phase deposition processes such as sputtering and ALD can directly form catalysts on anode but they are limited to produce small electrode, batch production. Furthermore, the cost for these systems is also an obstacle for commercial application.

The abundant and thus cheaper metal oxides such as Ti, Ta and Sn oxides have been successfully doped or alloyed into Ir oxides not only reduce the Ir content but also improve the catalytic activity and stability.² The improvement was believed to be due to the synergistic interaction of multicomponents by forming solid solution of mixed metal oxides.²

Silicon (Si) oxide is one of the most abundant materials in the earth's crust. It is inert and homogeneously disperses with other components in a mixture. Si oxide also possesses an amorphous structure that can improve the surface area of active components. Because of these advantages, doping Si oxide onto Ir oxides may improve the catalytic activity and stability.

In the previous works, Si oxide has been doped into Ir oxide to enhance the long-term stability of Si oxide-doped Ir oxides,^{3a,b,c} unfortunately, it has not yet been able to enhance the catalytic activity beyond that of Ir oxides. The Si oxide-doped Ir oxide film was prepared by the thermal decomposition of a mixture of hexachloroiridate (H_2IrCl_6) and tetraethoxysilane (TEOS) in alcohol under air at 500 °C. The decreased catalytic activity of this film may be due to Si oxide does not form alloys or solid solutions with Ir oxide in the mixture Si oxide-Ir oxide.^{3b} The film contains two different phases, crystal Ir oxide and amorphous Si oxide. In order to enhance both catalytic activity and long-term stability as well as reduce the Ir content by doping Si

oxide, a new preparation method that can form solid solutions with the highly homogeneous distribution of Ir oxides and Si oxide is required.

3.2.3. Strategy to resolve the obstacles

As discussed above, the decreased catalytic activity of the previous work is due to Si oxide does not form alloys or solid solutions with Ir oxides. To enhance both catalytic activity and stability as well as reduce the Ir contents by doping Si oxide, we need to develop a new preparation method that is able to form solid solutions. The following strategies may solve this problem.

An iridium complex with direct Ir-Si bond may be a potential molecular precursor. The direct Ir-Si bond may form a solid solution of Si oxide-doped Ir oxides with the highly homogeneous distribution of Ir and Si components due to the molecular interaction between Ir and Si atom.

Regarding preparation methods, the gas phase deposition approach is desirable because it does not involve using solvents like wet chemistry processes thus, it can prevent the aggregation of metals when as the solvents are removed. If we use gas phase deposition process, the catalyst will be deposited directly onto electrode instead of the numerous necessary steps required in conventional methods.^{1d} The MOCVD method may satisfy the requirement.

With aforementioned reasons in mind, the author attempts to prepare a Si oxide-doped Ir oxide by MOCVD using a volatile organometallic complex with direct Ir-Si bond as a precursor.

The Ir-Si complex, $[\text{Ir}^{\text{V}}(\eta^5\text{-C}_5\text{Me}_5)(\text{H})_2(\text{SiEt}_3)_2]$ (**2**) (Figure 3.3) was first synthesized by Maitlis and co-workers.⁶ This air and moisture-stable complex has two steric triethylsilyl $\{\text{Si}(\text{Et})_3\}$ and two hydride ligands those render it high volatility. However, this complex has not been used for MOCVD. In this work, the author

employs this complex as a MOCVD precursor to prepare a Si oxide-doped Ir oxide film for water oxidation catalyst.

It is important to note that amorphous Ir oxide is of interest because it obtains higher catalytic activity for water oxidation since it offers structural flexibility and the larger density of unsaturated sites.

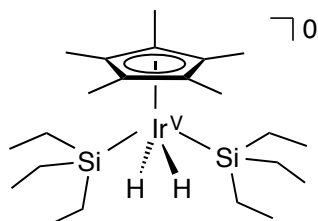


Figure 3.3 Chemical structure of Ir-Si complex, $[\text{Ir}^{\text{V}}(\eta^5\text{-C}_5\text{Me}_5)(\text{H})_2(\text{SiEt}_3)_2]$ (**2**)

3.2. RESULTS AND DISCUSSION

3.2.1. Thermal properties of precursor **2**

An Ir-Si complex $[\text{Ir}^{\text{V}}(\eta^5\text{-C}_5\text{Me}_5)(\text{H})_2(\text{SiEt}_3)_2]$ (**2**) was synthesized according to the literature procedure.⁶ In order to test the suitability of **2** as a MOCVD precursor, its thermal properties were investigated by thermogravimetry-differential thermal analysis (TG-DTA) (Figure 3.4). The measurement was carried out under nitrogen gas with the flow rate of 200 standard cc min⁻¹ (sccm) at a linear heating rate of 2.0 °C min⁻¹ under atmospheric pressure. The TG curve shows a single step weight loss between 130 °C and 250 °C with minimal residual (< 5 wt %), indicating high volatility and good thermal stability. The DTA curve shows a sharp peak at 82 °C without weight loss in TG curve that corresponds to the melting point. These thermal properties indicate that complex **2** is an excellent precursor for MOCVD.

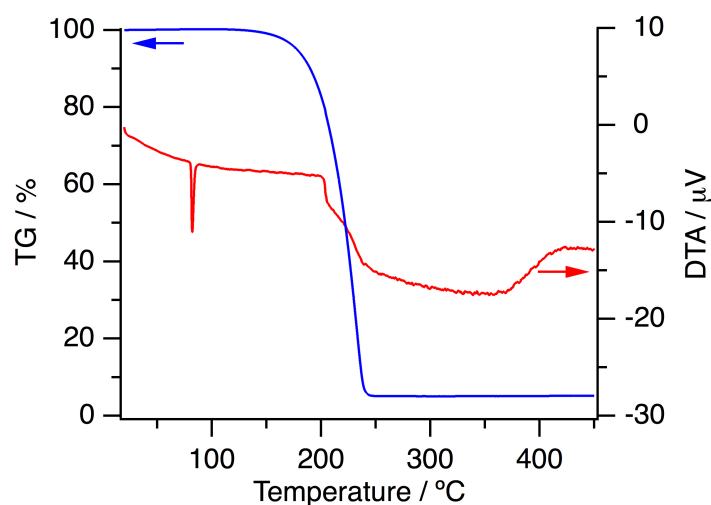


Figure 3.4 TG-DTA analysis of Ir^V complex, $[\text{Ir}^{\text{V}}(\eta^5\text{-C}_5\text{Me}_5)(\text{H})_2(\text{SiEt}_3)_2]$ (**2**) (flow gas: N₂, flow rate: 200 sccm, heating rate: 2.0 °C min⁻¹).

3.2.2. Preparation and characterization of IrSi oxide thin film

A Si oxide-doped Ir oxide film (IrSi oxide film, film **F₂**) was prepared through two steps. First, the Si oxide-doped Ir metal film (film **F₁**) was deposited on a fluorine doped tin oxide (FTO) substrate by MOCVD using complex **2** as a single-source precursor. Second, **F₁** is oxidized by electrochemical treatment to afford the Si oxide-doped Ir oxide film (IrSi oxide film, film **F₂**) (Figure 3.5).

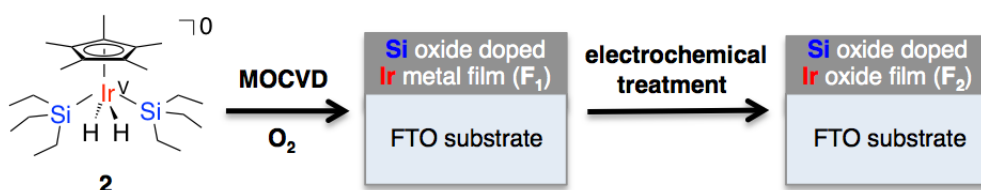


Figure 3.5 Formation of Si oxide-doped Ir oxide film (IrSi oxide film, film **F₂**) on FTO substrate by using complex **2** as a single precursor.

The MOCVD process was carried out using a tube type CVD apparatus with O₂ as the carrier or reactive gas. The complex **2** was vaporized at 95 °C under the pressure of 55-60 Pa with 40 sccm of O₂ gas while the temperature of FTO substrate was varied in the range of 350-450 °C. The optimized deposition condition was obtained at 400 °C.

The surface of the deposited film **F₁** was then oxidized by electrochemically cycling from -0.3 to +1.5V vs Ag/AgCl using 0.5 M H₂SO₄/H₂O (pH 0) as the electrolyte. The treatment was continued until the current density at the potential of 1.5 V reaches a saturated value to afford film **F₂** (Figure 3.6). This electrochemical oxidization of metallic Ir into active Ir oxide has been reported for Ir thin film and IrNi oxide nanoparticles.⁶

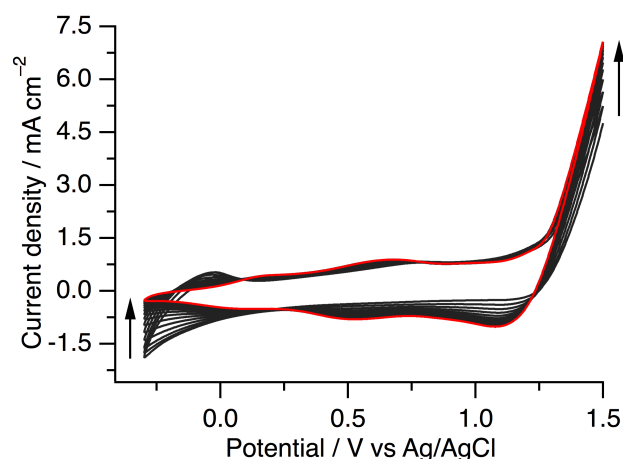


Figure 3.6 Cyclic voltammograms during conversion of film **F₁** to film **F₂** in 0.5. M H₂SO₄/H₂O at room temperature with scan rate of 100 mV s⁻¹. Film **F₂** on FTO substrate, Pt wire and Ag/AgCl were used as the working electrode, the counter electrode and the reference electrode, respectively.

In order to characterize film **F₁** and **F₂**, several measurements were carried out: X-ray photoelectron spectroscopy (XPS), scanning transmission electron microscopy (STEM) equipped energy dispersive X-ray spectroscopy (EDS) mappings, scanning electron microscopy (SEM) and X-ray diffraction (XRD) spectroscopy.

The compositions at the surface and the deep layer of film **F₁** and **F₂** were determined by XPS measurements.

Figure 3.7 shows the XP spectrum of film **F₁** before being etched by sputtering with Ar ions. The peaks originating from Ir, Si and O elements were observed. The binding energies of Ir 4f_{7/2} and Ir 4f_{5/2} are 61.3 eV and 64.3 eV, respectively which correspond to those found for metallic Ir⁰ (Figure 3.7 (C)). These results elucidated that the surface of film **F₁** contains metallic Ir and Si oxide. After being etched by sputtering with Ar ions until the peaks derived from tin (Sn) of FTO substrate appeared, the peaks of Ir, Si and O elements still remained and the Ir peaks of Ir 4f_{7/2}

and Ir 4 $f_{5/2}$ were not changed (Figure 3.7 (D)), meaning a uniform distribution of Ir, Si and O at the outside and inside of film **F**₁.

The XP spectrum of film **F**₂ before sputtering shows the peaks originated from Ir, Si and O (Figure 3.8). The binding energies of Ir 4 $f_{7/2}$ and Ir 4 $f_{5/2}$ are 61.9 and 63.9 eV, respectively (Figure 3.8 (C)), which correspond to those of Ir oxide.^{7c} After sputtering by Ar ions, these peaks shifted to 60.9 and 63.9 eV, respectively (Figure 3.8 (D)), which correspond to those found for metallic Ir. These results revealed that the metallic Ir near the surface was oxidized to Ir oxide by electrochemical treatment. Film **F**₂ has a Si oxide-dope Ir oxide layer at the surface while its deep layer is Si oxide-dope Ir metal.

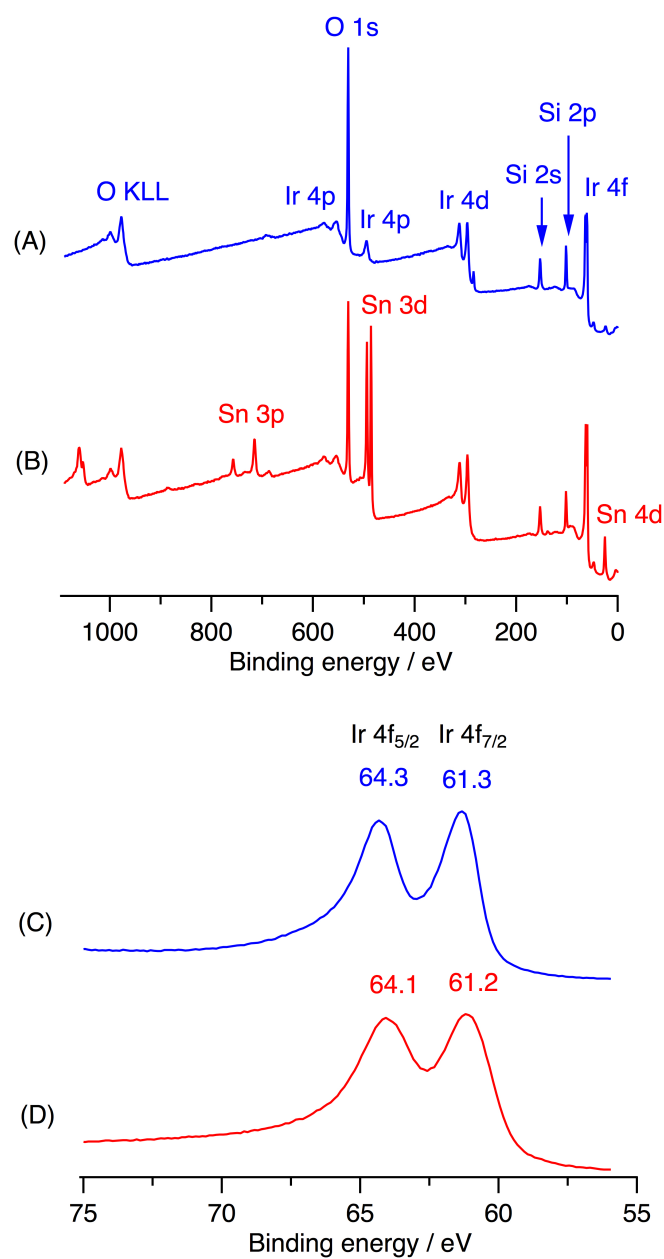


Figure 3.7 XPS results of the film **F₁** on FTO substrate: (A) before and (B) after being etched by sputtering with Ar ions. Magnifications of Ir 4f_{7/2} and Ir 4f_{5/2} peaks (C) and (D) in the spectrum (A) and (B), respectively.

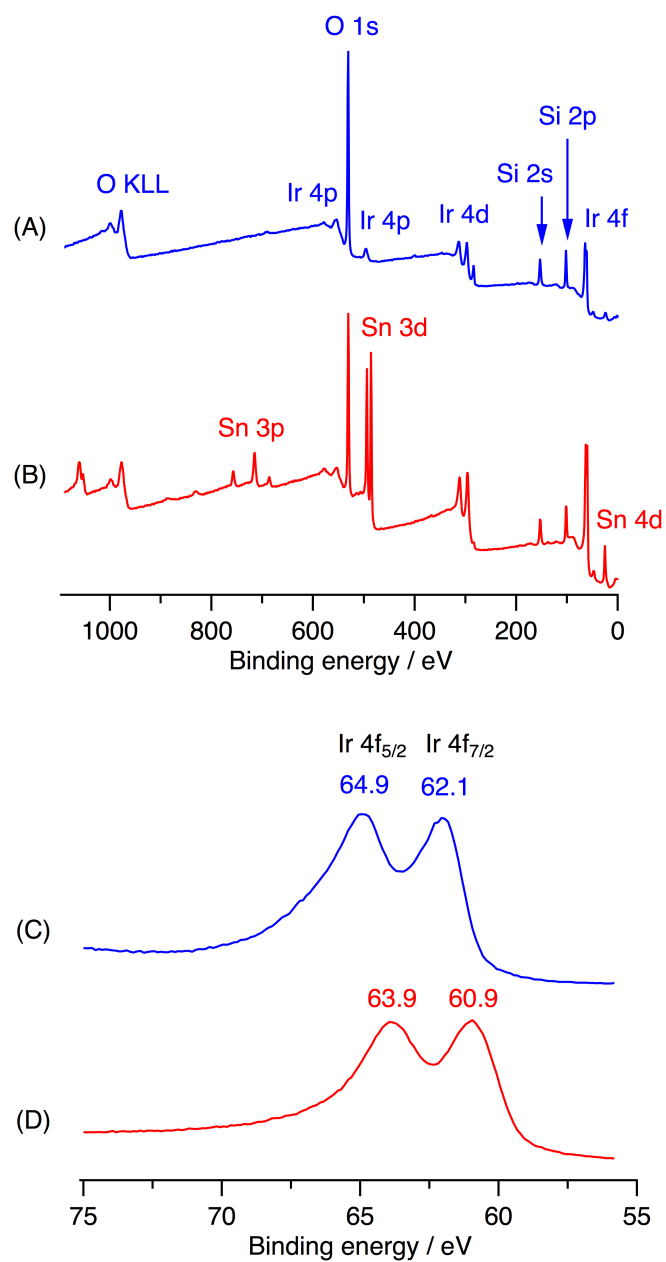


Figure 3.8 XPS results of the film F_2 on FTO substrate: (A) before and (B) after being etched by sputtering with Ar ions. Magnifications of Ir 4f_{7/2} and Ir 4f_{5/2} peaks (C) and (D) in the spectrum (A) and (B), respectively.

Figure 3.9 shows the line-profiles of Ir, Si and O elements by STEM-EDS of film **F**₁ and **F**₂. For film **F**₁, the relative composition of Ir, Si and O at the surface and in deep layer are similar, suggesting a uniform distribution of these components. For the film **F**₂, the relative component of O at the surface increased while relative component of Ir and Si. The atomic ratios of Ir: Si: O for film **F**₂ at surface and deep layer are estimated as 15:23:62 and 19:31:50, respectively. This means electrochemical treatment converts Ir metal at surface into Ir oxide. The surface of film **F**₂ contains Ir oxide and Si oxide and the deep of layer is a mixture of Ir metal and Si oxide. The result is consistent well with the evident given by XPS.

The Ir contents of film **F**₂ at the outside and inside are 15 and 19 % respectively those are lower than pure Ir oxide film.

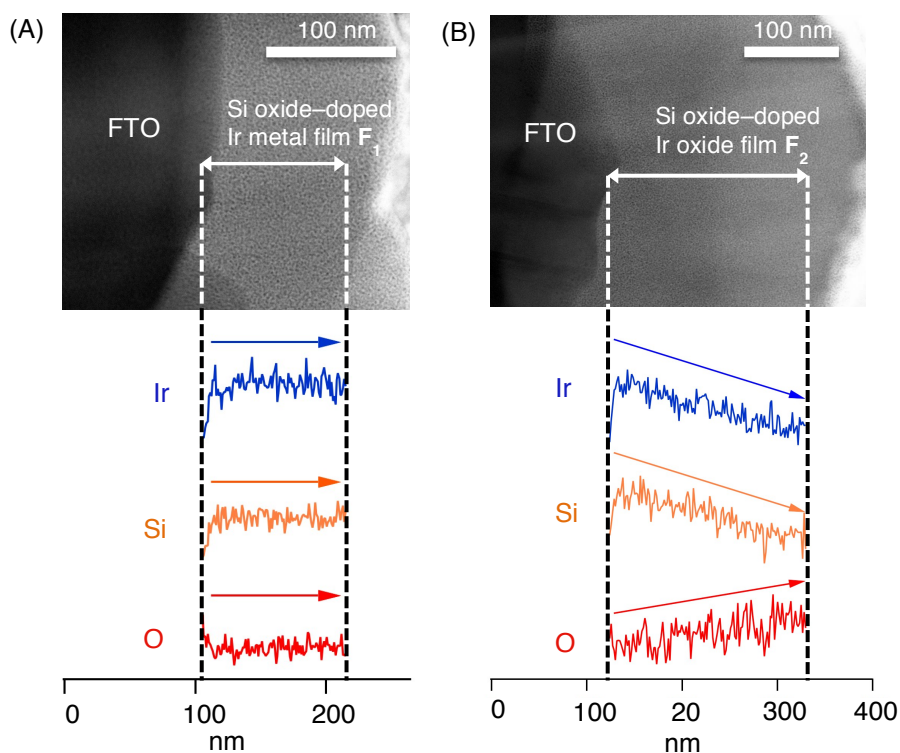


Figure 3.9 STEM images of (A) film **F**₁ on FTO substrate, (B) film **F**₂ on FTO substrate with line-profiles of Ir (blue), Si (orange) and O (red) atoms.

The elemental distribution maps of film F_1 and F_2 were obtained by STEM-EDS (Figure 3.10 and 3.11, respectively). These images show a uniform distribution of Ir, Si and O elements for both film F_2 and F_1 . This result confirmed that MOCVD of complex **2** offers a solid solution film with homogenous distribution of Ir oxide and Si oxide

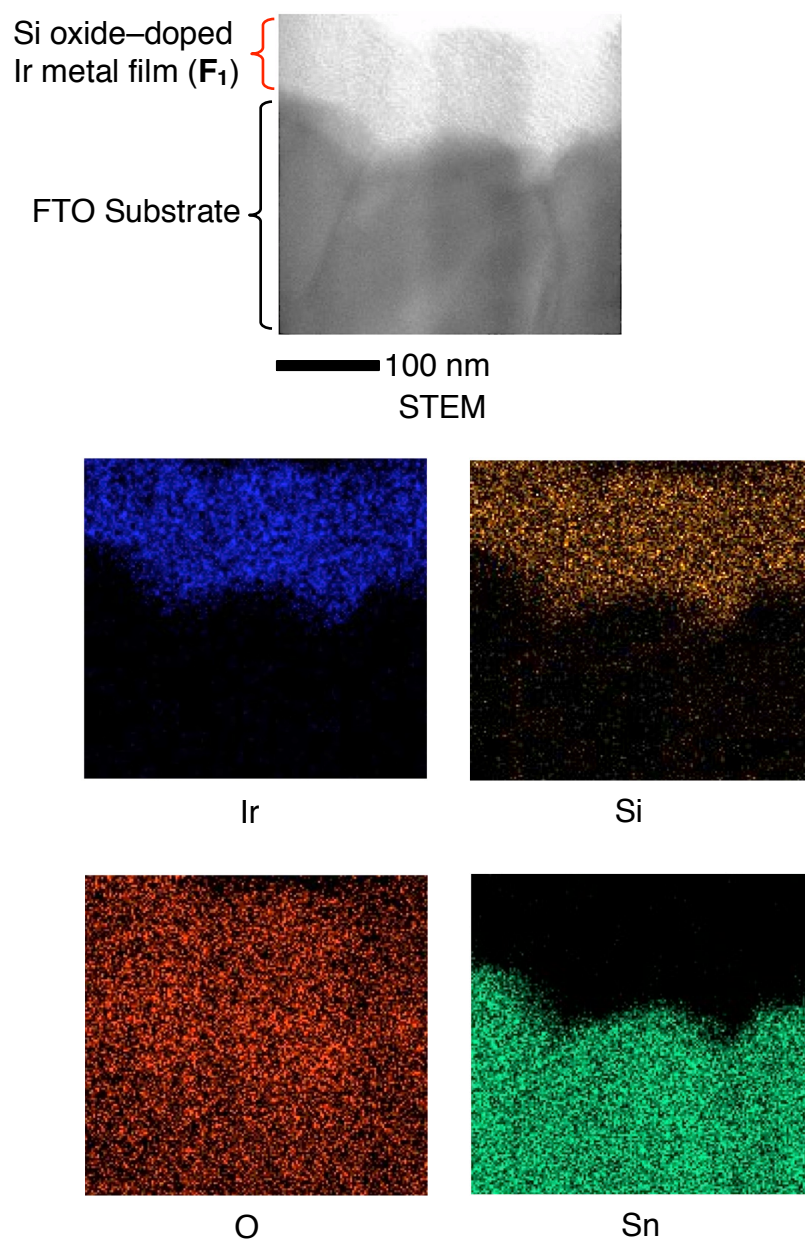


Figure 3.10 STEM image of film F_1 on FTO substrate with elemental mappings for Ir (blue), Si (orange), O (red) and Sn (green)

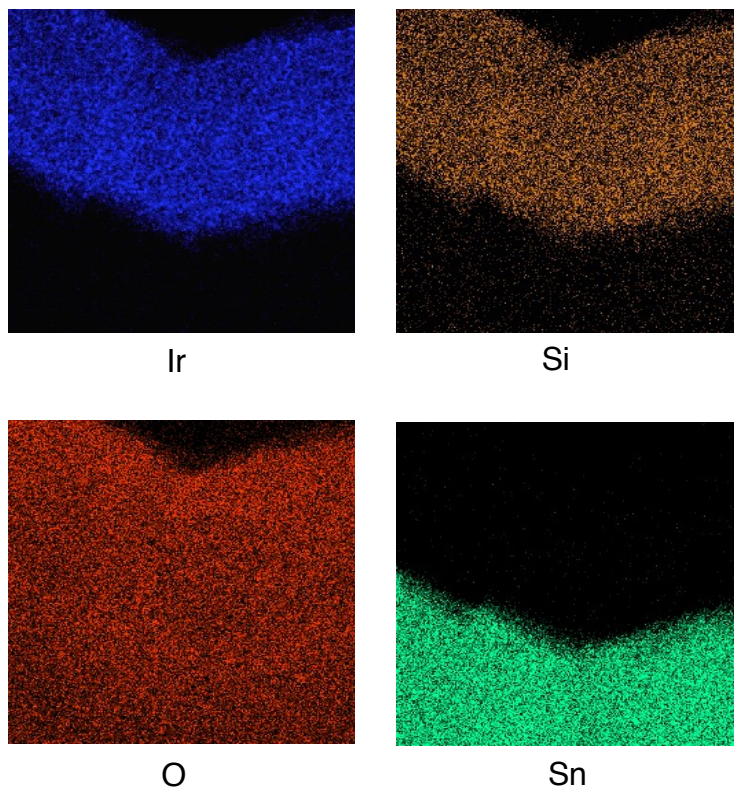
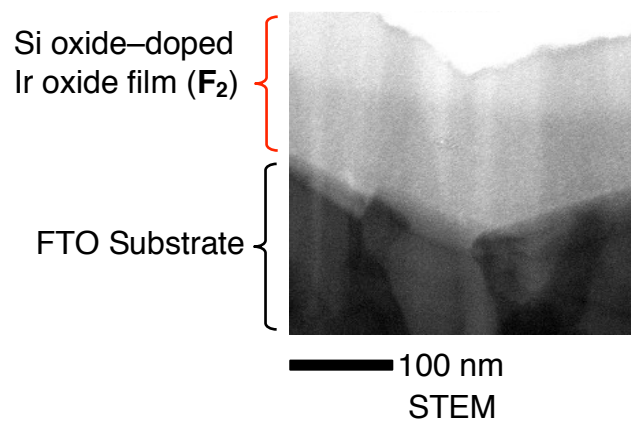


Figure 3.11 STEM image of film F_2 on FTO substrate with elemental mappings for Ir (blue), Si (orange), O (red) and Sn (green).

The SEM measurements were conducted to investigate the morphology of film **F**₁ and **F**₂. Figure 3.12 shows SEM images of bare-FTO substrate, films **F**₁ and **F**₂ that revealed amorphous particles of both films **F**₁ and **F**₂. The particles morphology is not affected by the electrochemical oxidization.

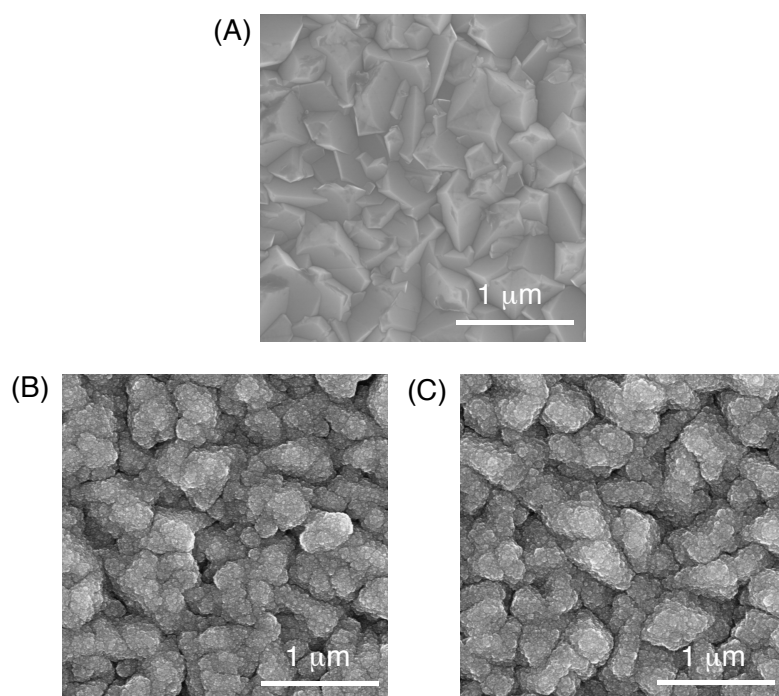


Figure 3.12 SEM images of (A) bare-FTO substrate, (B), the film **F**₁ on FTO substrate and (C) the film **F**₂ on FTO substrate.

As previously mentioned, the amorphous phases of metal oxides are preferable owing to their superior electrocatalytic water oxidation. To confirm the amorphous state of film **F**₁ and **F**₂, X-ray diffraction (XRD) spectroscopy were performed. XRD spectra of films **F**₁ and **F**₂ on FTO substrate show only the diffraction peaks originated from the Sn oxide of FTO substrate, implying the amorphous phase of these films (Figure 3.13 (A), (B) and (C)). In some cases, the diffraction peak does not appear in XRD spectra if the film is too thin or the amount of crystal is too small. To eliminate this possibility, the post-XRD-measurement film **F**₂ is annealed to induce crystallization and then XRD measurement is carried again. After heating at

600 °C for 2 h, the diffraction peaks originated from Ir oxide were observed, revealing the amorphous phase of film **F**₂ before heating (Figure 3.13 (D)).

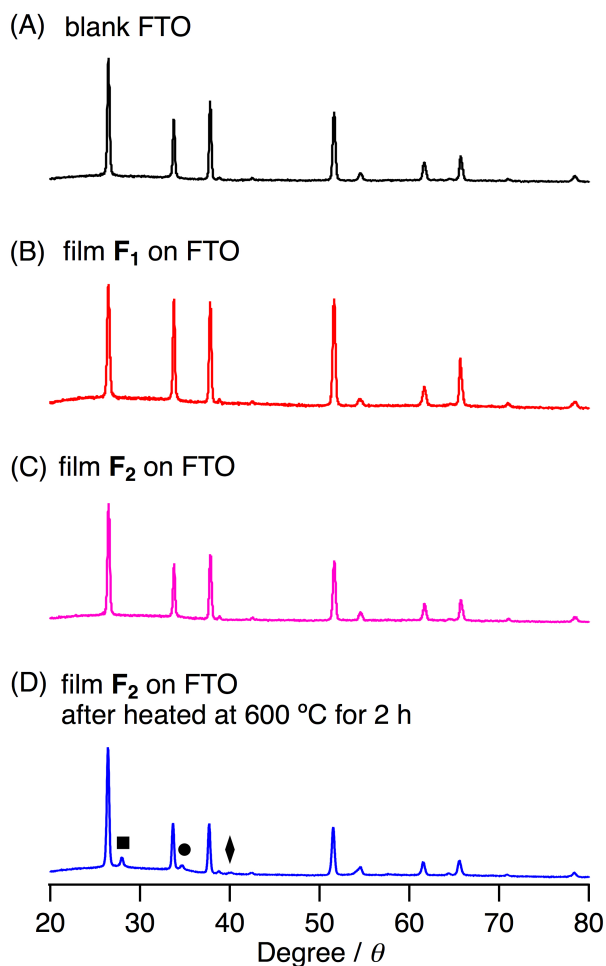


Figure 3.13 X-ray diffraction patterns of (A) bare-FTO substrate, (B) the film **F**₁ on FTO substrate (C) the film **F**₂ on FTO substrate and (D) the film **F**₂ on FTO substrate was heated at 600 °C for 2 h.

3.2.3. Electrochemical behaviors of IrSi oxide film

First, the water oxidation of film **F₂** was investigated in acidic condition. Cyclic voltammetry (CV) was conducted using film **F₂** on FTO substrate as a working electrode, Pt wire as a counter electrode and Ag/AgCl as a reference electrode at pH 0 in 0.5 M H₂SO₄/H₂O. The CV is shown in Figure 3.14. The current density increases significantly at the potential around 1.2 V vs Ag/AgCl with evolving gas bubbles, which is the catalytic current of water oxidation.

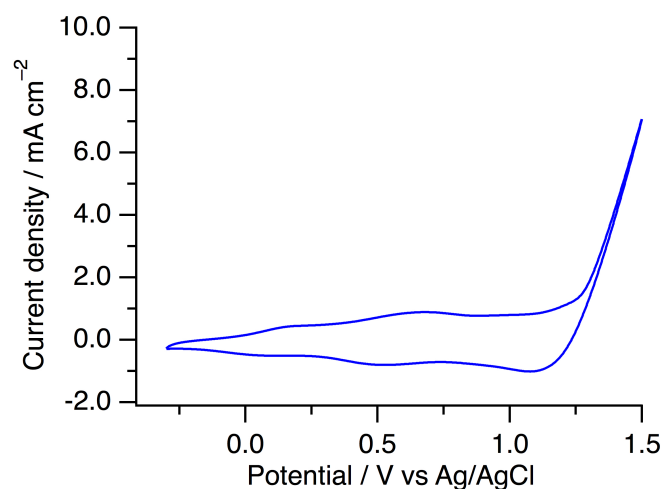


Figure 3.14. Cyclic voltamogram of film **F₂** on FTO substrate at pH 0 in 0.5 M H₂SO₄/H₂O at 100 mV s⁻¹

The evolving gas at anode during CV measurement was identified to be oxygen (O₂) by gas chromatography-mass spectrometry (GC-MS). To confirm the O₂ gas originated from water, an isotope-labeling experiment was conducted using labeled water (H₂¹⁸O). ¹⁸O-labeled dioxygen gases (^{16,18}O₂ and ¹⁸O₂) were evolved and identified by GC-MS during electrochemical water-oxidation by film **F₂** at pH 0 in 0.5 M H₂SO₄/H₂O containing 5% H₂¹⁸O (Figure 3.15). The ¹⁸O atom ratio of 5.4 % in the evolved gases (¹⁶O₂, ^{16,18}O₂ and ¹⁸O₂) is consistent to theoretical value of 5.1 %. These results clearly confirmed that film **F₂** functions as a water-oxidation catalyst.

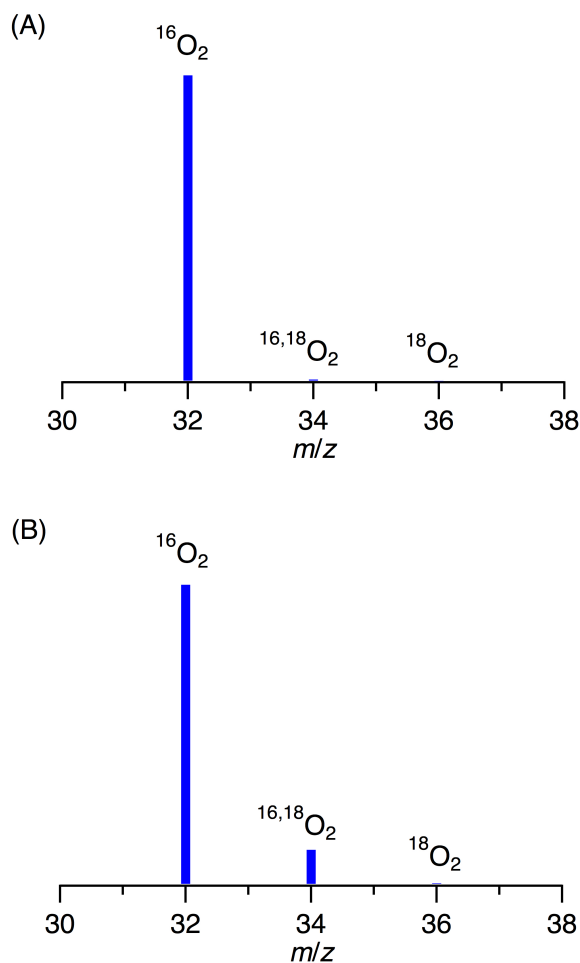


Figure 3.15 Positive-ion GC mass spectra of the gas obtained from the electrochemical water-oxidation by the film **F₂** on FTO substrate at pH 0 in 0.5 M H₂SO₄/H₂O, (A) using normal H₂O, (B) using 5% labeled H₂¹⁸O.

The water oxidation of the film **F₂** was also investigated at different pH in range of 0-13 (Figure 3.16). The potentials were corrected for the Ohmic drops that were measured by impedance spectra (Figure 3.22, experiment section).

The pH dependent potentials for water-oxidation reaction by film **F₂** were studied, in which each potential was determined at 0.5, 1.0 and 1.5 mA cm⁻² (Figure 3.16 (B)). The slopes are about 59 mV per pH, which means that the reaction

proceeds with one electron paired one proton. This matches the pairing of four electrons and four protons for water oxidation reaction.

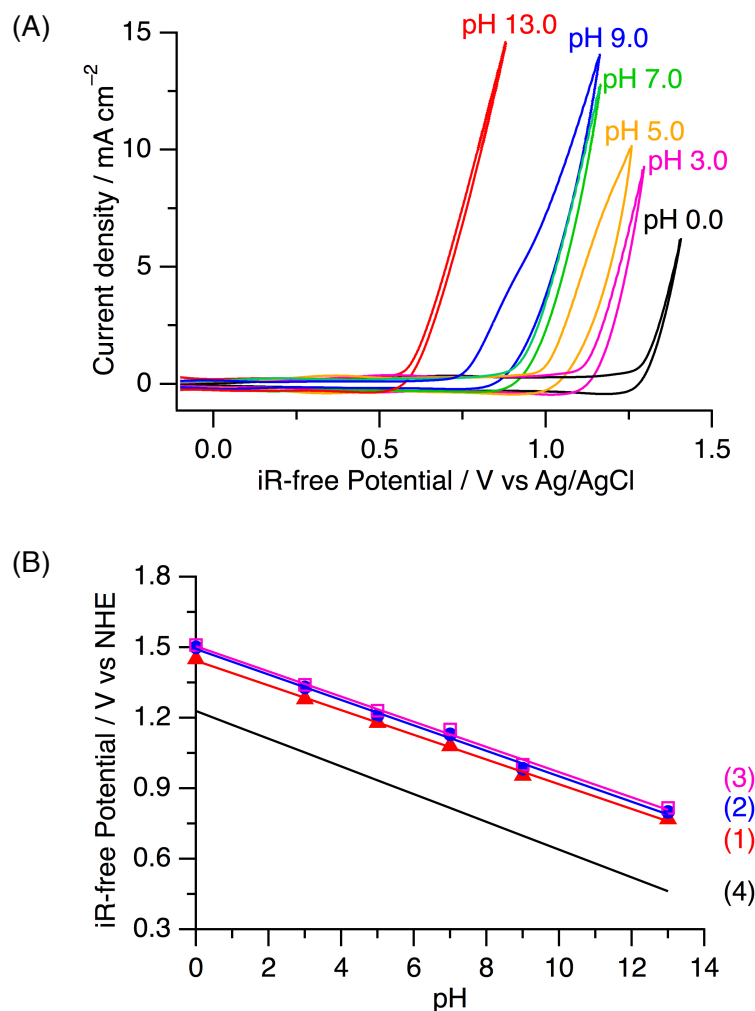


Figure 3.16 (A) Cyclic voltammogram of the film F_2 on FTO substrate in aqueous solutions in the pH range of 0.0-13.0 at 100 mV s^{-1} (B) Plots of pH against iR-free potential determined by CV measurements of the film F_2 on FTO substrate at (1) 0.5 mA cm^{-2} , (2) 1.0 mA cm^{-2} , (3) 1.5 mA cm^{-2} . (4) A plot of pH against thermodynamic potential for water oxidation

In the ideal condition, the thermodynamic water-oxidation potential at pH 0 is 1.299 V vs NHE . However, in practical conditions, there are some thermodynamic

losses. An extra potential is needed to overcome these thermodynamic losses, we call this extra potential is overpotential.

The overpotential for film **F₂** at pH 0, at a current density of 0.5 mA cm⁻² (at room temperature) was determined as 0.22 V. This value is comparable to those reported for other Ir oxide-based catalysts (overpotential = 0.20-0.28 V at the current density of 0.5 mA cm⁻² at pH 0).

Figure 3.17 shows the Tafel plots of film **F₂** for water oxidation in aqueous solutions in the pH range of 0-13. The Tafel slopes for pH 0, 3, 5, 7, 9 and 13 were determined as 141, 176, 211, 274, 318 and 416 mV/decade, respectively. The Tafel slopes increase with increment of the pH values. This means film **F₂** has better water-oxidation catalytic activity in acidic media.

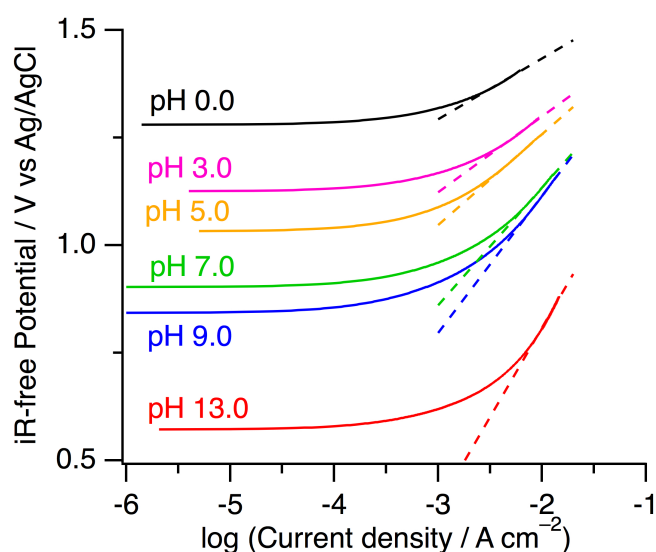


Figure 3.17 Tafel plot of film **F₂** on FTO substrate for water oxidation in aqueous solutions in the pH range of 0-13.

The Tafel slopes of **F₂** are higher than those reported for the Ir-based catalysts (40-60 mV/decade). The high value of Tafel slopes is probably due to poor current collection ability, which is attributable to the low electric conductivity of film **F₂**. Because film **F₂** contains inert Si oxide, it is expected to have lower electronic

conductivity than the pure Ir oxide films. The intensive bubbles or strong absorption of gaseous O_2 at anode surface (film **F**₂) during the measurement also resulted in the high value of Tafel slopes.

Turn overfrequency (TOF) is the number of moles of evolved O_2 gas per moles of the electroactive Ir in a second. TOF is considered as the best option to evaluate the activity of a catalyst because it expresses the “per-site” activity.

To calculate TOF, we have to determine the moles of electroactive Ir and the moles of evolved O_2 gas. The moles of electroactive Ir on film **F**₂ were estimated according to the literatures from the anodic wave of Ir^{III}/Ir^{IV} observed in cyclic voltammograms. The evolved O_2 gas was collected by water displacement method and then the mol of O_2 was calculated based on the volume, pressure and temperature of the gas. The detailed procedures are described in the experimental section.

TOFs for electrochemical water-oxidation at pH 0 (H_2SO_4/H_2O) were measured at several potentials using film **F**₂ on FTO substrate as a working electrode for 30 min. The iR-free potential dependent TOFs at pH 0 are shown in Figure 3.18.

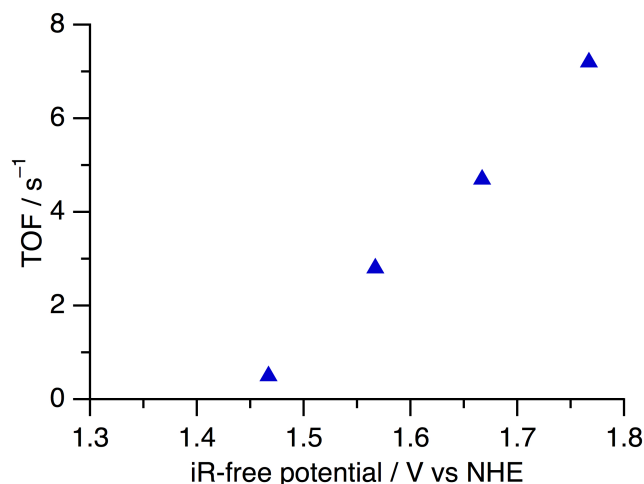


Figure 3.18 A plot of TOF vs iR-free potential for water oxidation by the film **F**₂ at pH 0 in 0.5 M H_2SO_4/H_2O at room temperature.

The TOFs of film **F₂** at iR-free potential of 1.76, 1.66, 1.56 and 1.46 V vs NHE were determined as 7.2, 4.7, 2.8 and 0.5 s⁻¹, respectively.

In order to compare the catalytic activity of film **F₂** with Ir oxide film, an Ir oxide film on FTO was made according to literature,^{4c} which is described in the experimental section. The TOF of the Ir oxide film was determined using the same procedure for film **F₂**.

The TOF at iR-free potential of 1.76 V vs NHE for the electrochemical water-oxidation at pH 0 was 7.2 s⁻¹ higher than the value of 2.5 s⁻¹ for the Ir oxide film.

The catalytic activity of film **F₂** was also investigated in neutral condition. The TOF at iR-free potential of 1.36 V vs NHE for the electrochemical water-oxidation at pH 0 was 5.3 s⁻¹. This value is comparable with those reported for other Ir oxide-based catalysts^{5c} and slightly lower than the highest reported value of 8.0 s⁻¹ for the Ir oxide film.^{5f} The result is reasonable because film **F₂** is more active for water oxidation in acidic media than in basic regime.

Along with high activity, the stability or service life of the catalyst is another important factor for practical application. In order to test the stability of film **F₂**, chronopotentiometric measurement was conducted at the current density of 1.0 mA cm⁻² in 0.5 M H₂SO₄/H₂O (pH 0) at room temperature for 24 h (Figure 3.19). The potential remained constant throughout the test duration of 24 h, which indicates the stable behavior of film **F₂** in strong acidic condition.

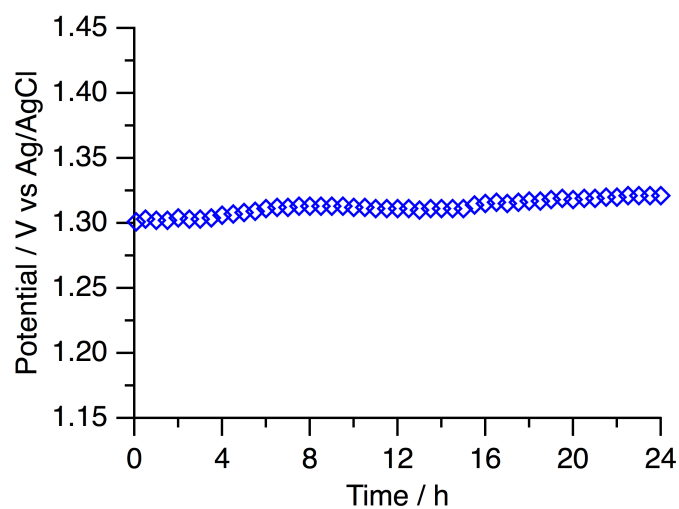


Figure 3.19 Chronopotentiometric measurement of the film \mathbf{F}_2 in 0.5 M $\text{H}_2\text{SO}_4/\text{H}_2\text{O}$ (pH 0) at room temperature, potential required maintaining a 1 mA cm^{-2} current density. The film \mathbf{F}_2 on FTO substrate, Pt wire and Ag/AgCl were used as the working electrode, the counter electrode and the reference electrode, respectively.

3.3. CONCLUSION

In conclusion, a novel IrSi oxide film has been prepared by MOCVD using an iridium-silyl complex as a single precursor and successive electrochemical oxidization. The amorphous IrSi oxide film exhibited high catalytic activity and stability for water oxidation in acidic media. The turnover frequency (TOF) for water oxidation in acidic media was determined giving a higher value than those reported for Si oxide-doped Ir oxide and higher even than pure Ir oxide. This work has succeeded in doping Si oxide into Ir oxide to reduce Ir contents as well as enhance catalytic activity and stability using a novel preparation strategy. The author believes the analogous organometallic compounds with direct metal-silyl bonds will be promising single MOCVD precursors that are able to form highly homogeneous Si oxide-doped metal oxide films for applications not only in catalyst but also in other fields.

3.4. EXPERIMENTAL

3.4.1. Materials and Methods

All manipulations were performed under an N₂ gas using either standard Schlenk or glovebox techniques. An Ir^V complex [Ir^V(η⁵-C₅Me₅)(H)₂(SiEt₃)₂] (**2**) was synthesised following the literature method.⁶ A fluorine doped tin oxide (FTO) coated glass slide (Type VU) was purchased from AGC Fabritech Co., Ltd. Distilled water was purchased from Wako Pure Chemical Industries, Ltd. H₂¹⁸O (98 atom%) was purchased from TAIYO NIPPON SAN SO CO., Ltd. All other chemicals were obtained from commercial sources and used as received.

The scanning electron microscopy (SEM) measurement was performed using a Hitachi SU8000. X-ray photoelectron spectroscopy (XPS) was obtained by an ULVAC PHI 5000 VersaProbe II system with an Al anode X-ray source. Binding energies were calibrated by Sn 3d_{5/2} peak of FTO substrate at 486.7 eV.⁸ In order to investigate the composition of catalyst film at deep layer, Ar ion sputtering was used to etch surface of the catalyst layer. X-ray diffraction (XRD) patterns were observed by an X-ray diffractometer (Rigaku SmartLab) with Cu-Kα radiation generated at 40 kV and 30 mA {scan speed: 0.01° min⁻¹(2θ = 20-80 °C)}. Scanning transmission electron microscope (STEM) with energy dispersive X-ray spectroscopy (EDS) mappings was conducted using a JEOL JEM-ARM 200F with a silicon drift detector (SDD). Electrochemical measurement were carried out using ALS Electrochemical Analyzer Model 600D and 760DT. Impedance spectra were recorded on a TOYO Corporation Fuel Cell Test System 890CL and Solartron Models 1287A Potentiostat/Galvanostat and 1255B Frequency Response Analyzer. Gas chromatography mass spectrometry (GC-MS) was conducted using a SHIMADZU GCMS-QP 5050.

3.4.2. Thermal properties of complex 2

Thermal properties measurement was carried out under a flow of N₂ gas with a flow rate of 200 sccm by thermogravimetry–differential thermal analysis (TG–DTA) using an EXSTAR TG–DTA7300 instrument. 5 mg of complex **2** was loaded in an open–type aluminium crucible. The heating rate was set at 2.0 °C min^{−1} and the measurement was performed under atmospheric pressure.

3.4.3. Preparation of the IrSi oxide catalyst

Deposition of Si oxide-doped Ir metal film (film F₁) by MOCVD using complex 2 as precursor

The Si oxide-doped Ir metal film (film F₁) was deposited onto an FTO substrate using a tube type chemical vapor deposition (CVD) reactor with glass tube diameter of 4.0 cm. The distance between precursor **2** and the FTO substrate was ca. 5.0 cm. Precursor **2** was heated to vaporization at ca. 95 °C under a pressure of 55-60 Pa with a flow O₂ gas (flow rate: 40 sccm), while the FTO substrate was maintained at 400 °C. The deposited time was set to a period of 5 min.

Electrochemical oxidization of the Si oxide-doped Ir metal film (film F₁) to form Si oxide-doped Ir oxide film (film F₂)

Electrochemical treatment was performed using 0.5 M H₂SO₄/H₂O (pH 0) as electrolyte at room temperature. Film (F₁) on FTO substrate, Pt wire and Ag/AgCl were used as working electrode, counter electrode and reference electrode, respectively. The potential sweep from -0.3 to +1.5 V vs Ag/AgCl was continued until the current density at 1.5 V vs Ag/AgCl get stable to afford Si oxide-doped Ir

oxide film (film **F₂**). The film **F₂** was washed with distilled water and dry in air before use.

Estimating the composition of film **F₁** and **F₂**

The atomic ratio of Ir: Si: O elements for films **F₁** and **F₂** were estimated by EDS measurement. The results are as followings:

Film **F₁** (atm): Ir = 19 %, Si = 28 % and O = 53 %.

Outside of film **F₂** (atm): Ir = 15 %, Si = 23 % and O = 62 %

Inside of film **F₂** (atm): Ir = 19 %, Si = 31% and O = 50 %

3.4.4. Preparation of the Ir oxide to compare with film **F₂**

Ir oxide was prepared according to the literature method. The detailed procedures are as follows:

Spin casting a solution of iridium acetylacetonates ($\text{Ir}(\text{acac})_3$) in chloroform (5% w/w) on an FTO substrate at 3000 rpm for 60 s. Then the film was irradiated with UV light (185/254 nm) for 1 h. The film was annealed at 500 °C for 1 h in air affords an Ir oxide film of FTO.

3.4.5. Evaluation of electrochemical water-oxidation

Electrochemical water-oxidation using film **F₂** as catalyst

The cyclic voltammograms were measured using film **F₂** on FTO substrate as working electrode, Pt wire as counter electrode and Ag/AgCl as a reference electrode at room temperature with scan rate of 100 mV s⁻¹.

Isotope-labeling experiment for oxidation of H_2^{18}O using film **F₂**

The electrochemical water-oxidation using the film **F₂** on FTO as catalyst at 1.71 V vs NHE was carried out in 0.5 M $\text{H}_2\text{SO}_4/\text{H}_2\text{O}$ containing 5% H_2^{18}O (pH 0) at room temperature. The evolved gas from film **F₂** was identified to be dioxygen gases ($^{16}\text{O}_2$,

^{16,18} O₂ and ¹⁸O₂) by GC-MS. The experiment was performed in the same condition without H₂¹⁸O, 18-labelled dioxygen was not observed.

Determination of the mol of electroactive Ir on film F₂

The electroactive Ir on film F₂ on FTO was calculated according to the literature method using the charge under the anodic wave of Ir^{IV}/Ir^{III} from the cyclic voltammogram.⁹

Based on dependence of peak current at scan rates for Ir^{IV}/Ir^{III} at 0.78 V.

$$\text{slope} = \frac{n^2 \times F^2 \times A \times \Gamma}{4 \times R \times T}$$

where, n = number of electrons, F = Faraday's constant (C/mol), A = area of electrode (cm²), Γ = surface concentration of Ir (mol/cm²), R = ideal gas constant (J/mol K) and T = temperature (K).

slope determined by Figure 3.20 (B) = 3.10×10^{-3} (C²/J)

$$3.10 \times 10^{-3} \text{ (C}^2/\text{J)} = \frac{1^2 \times 96485^2 \text{ (C}^2/\text{mol}^2) \times \Gamma \text{ (mol/cm}^2\text{)}}{4 \times 8.314 \text{ (J/mol K)} \times 296 \text{ (K)}}$$

$$3.10 \times 10^{-3} \text{ (C}^2/\text{J)} = \frac{9309355225 \text{ (C}^2\text{cm}^2/\text{mol}^2) \times \Gamma \text{ (mol/cm}^2\text{)}}{9844 \text{ (J/mol)}}$$

$$\Gamma \text{ (mol/cm}^2\text{)} = \frac{3.10 \times 10^{-3} \text{ (C}^2/\text{J)} \times 9844 \text{ (J/mol)}}{9309355225 \text{ (C}^2\text{cm}^2/\text{mol}^2\text{)}}$$

$$= 2.56 \times 10^{-9} \text{ (mol cm}^{-2}\text{)}$$

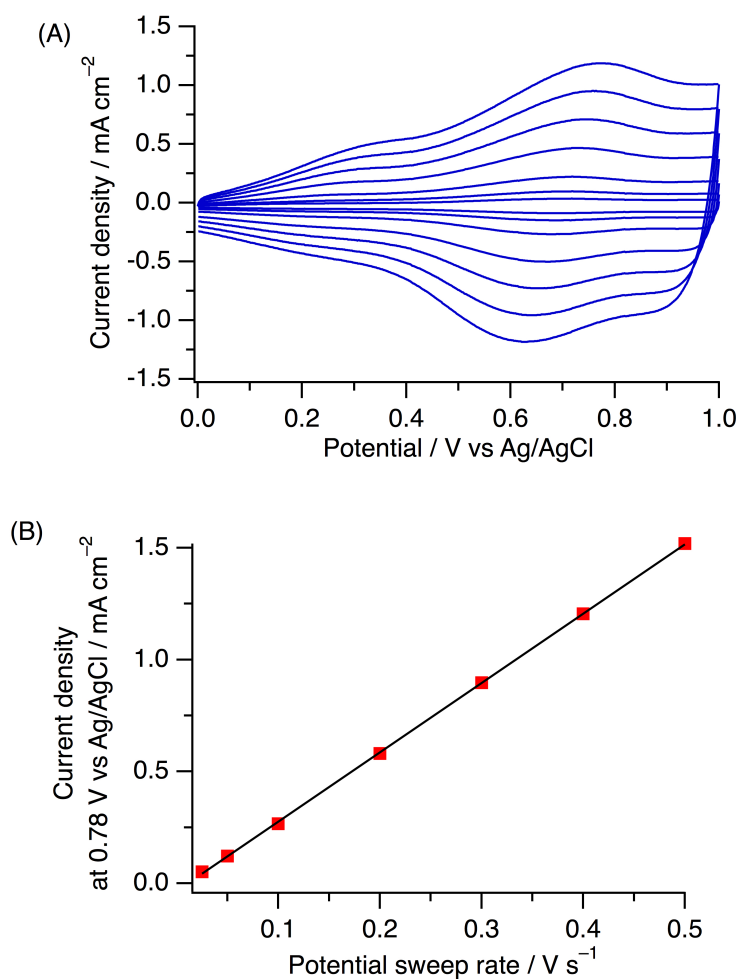


Figure 3.20 (A) Cyclic voltammograms of film **F₂** at different scan rates, (B) dependence peak current on different scan rates for $(\text{Ir}^{\text{IV}}/\text{Ir}^{\text{III}}) = 0.78 \text{ V}$

Calculation of turn over frequency (TOF) for water oxidation by film **F₂**

The film **F₂** on FTO substrate was used as a working electrode for water-oxidation at potentials from 1.61 to 1.91 V vs NHE for 30 min. at pH 0 in 0.5 M $\text{H}_2\text{SO}_4/\text{H}_2\text{O}$. The evolved O_2 gas was collected by water displacement method.

Ideal gas law: $PV = nRT$

where n = mol of gas (mol), P = pressure of gas, V = volume of gas, R = gas constant = 0.082 L atm/mol K, T = Kelvil temperature (K).

The mol of O_2 was determined for the case of 1.91 V vs NHE

$$\begin{aligned}
 n \text{ (mol)} &= \frac{P \text{ (atm)} \times V \text{ (L)}}{R \text{ (L atm/mol K)} \times T \text{ (K)}} \\
 &= \frac{1.0 \text{ (atm)} \times 0.80 \times 10^{-3} \text{ (L)}}{0.082 \text{ (L atm/mol K)} \times 296 \text{ (K)}} \\
 &= 3.30 \times 10^{-5} \text{ (mol)}
 \end{aligned}$$

The TOF was determined as follows.

$$\begin{aligned}
 \text{TOF} &= \frac{\text{mol of O}_2}{\text{mol of Ir}} \times \frac{1}{\text{time}} \\
 &= \frac{3.30 \times 10^{-5}}{2.56 \times 10^{-9} \times 1.0 \text{ (cm}^2\text{)}} \times \frac{1}{1800 \text{ (s)}} \\
 &= 7.2 \text{ (s}^{-1}\text{)}
 \end{aligned}$$

Determination of the mol of electroactive Ir on Ir oxide film and calculation the TOF for water oxidation by Ir oxide at pH 0

The mol of electroactive Ir on Ir oxide was determined using similar method for F_2 giving a value of $1.85 \times 10^{-9} \text{ (mol cm}^{-2}\text{)}$ (Figure 3.21). Then the TOF for electrochemical water-oxidation at 1.91 vs NHE was calculated giving the TOF value of 2.5 s^{-1} .

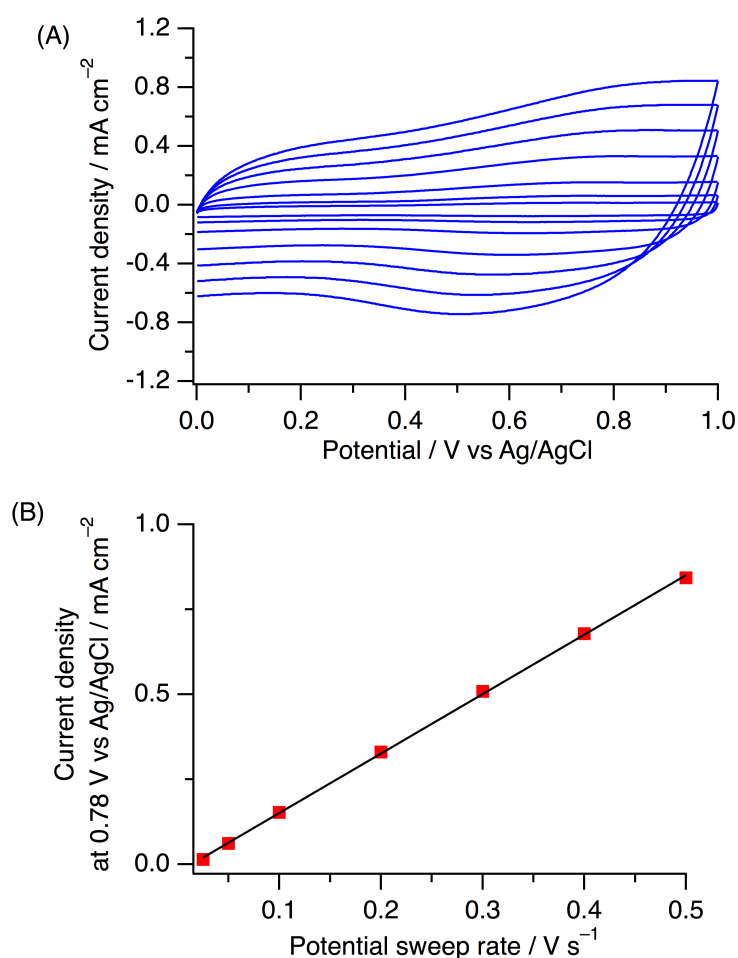


Figure 3.21 (A) Cyclic voltammograms of Ir oxide film at different scan rates, (B) dependence peak current on different scan rates for $(\text{Ir}^{\text{IV}}/\text{Ir}^{\text{III}}) = 0.78 \text{ V}$

Impedance measurement

A TOYO Corporation Fuel Cell Test System 890CL and Solartron Models 1287A Potentiostat/Galvanostat and 1255B Frequency Response were employed to measure the impedance. The 3-electrode, RE, WE and CE were connected to Ag/AgCl reference electrode, the **F2** film and Pt, respectively. An iR -free potential is calculated by the following equation

$$\text{potential} = V - iR$$

where V is voltage, i is current density and R is Ohmic resistance that is determined by each impedance measurement at pH 0–13 as shown in Figure 3.22. These spectra were measured under open-circuit conditions by changing the frequency from 0.1 to 1000 Hz. Black solid lines are curve fittings as a following circuit. Based on these fitting results, the Ohmic resistances are determined as 14.9, 21.9, 23.8, 26.1 24.0 and 42.4 cm^2 for pH

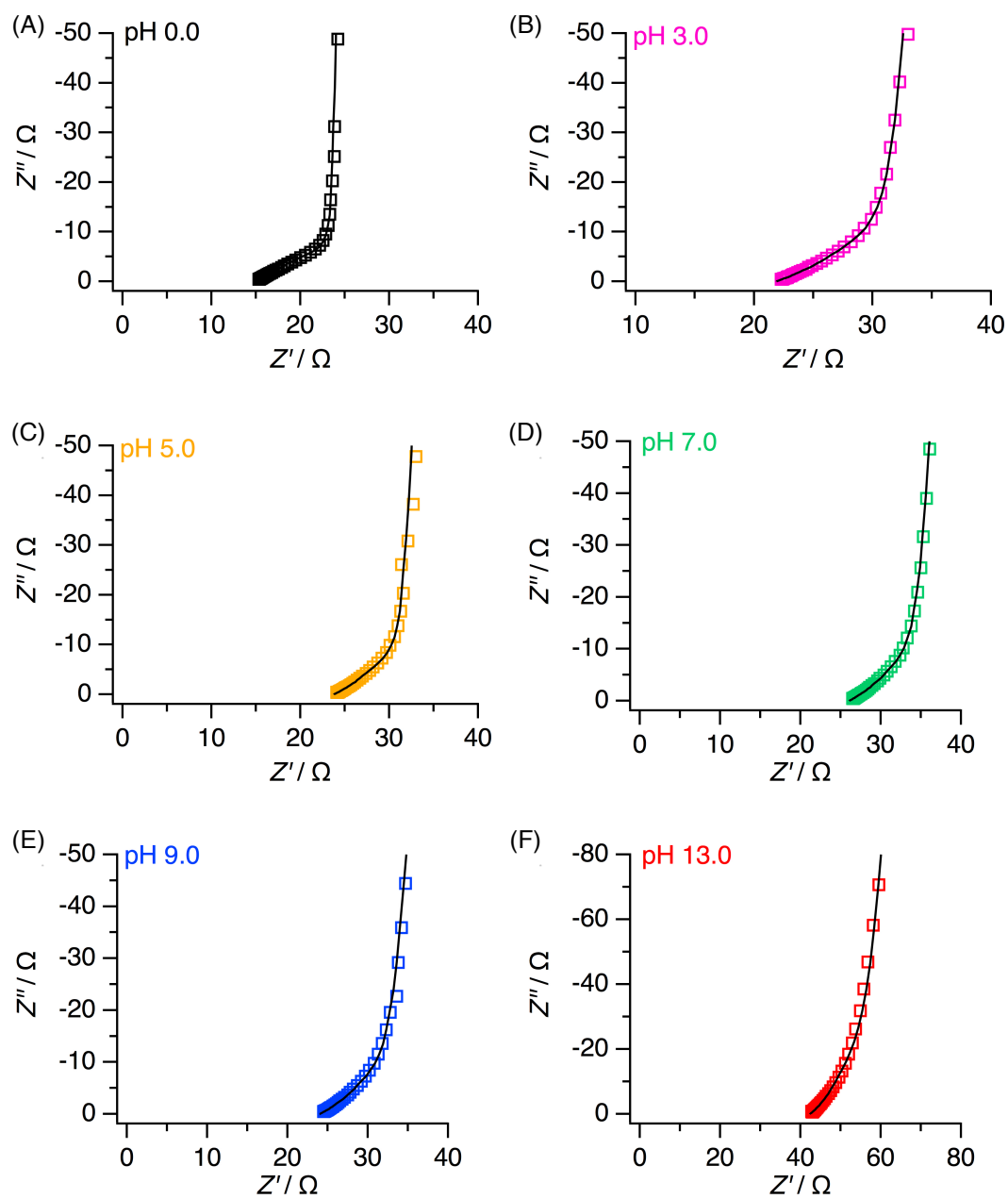


Figure 3.22 Impedance spectra of water oxidation by film F_2 in aqueous solution at various pH values. (A) pH 0, (B) pH 3, (C) pH 5, (D) pH 7, (E) pH 9 and (F) pH 13

REFERENCES

1. (a) I. Katsounaros, S. Cherevko, A. R. Zeradjanin and K. J. J. Mayrhofer, *Angew. Chem. Int. Ed.*, 2014, **53**, 102–121; (b) E. Antolini, *ACS Catal.*, 2014, **4**, 1426–1440; (c) J. R. Mckone, N. S. Lewis and H. B. Gray, *Chem. Mater.*, 2014, **26**, 407–414; (d) M. Carmo, D. L. Fritz, J. Mergel and D. Stolten, *Int. J. Hydrogen Energy*, 2013, **38**, 4901–4934; (e) S. Park, Y. Shao, J. Liu and Y. Wang, *Energy Environ. Sci.*, 2012, **5**, 9331–9344.
2. (a) Z. Yan, Y. Zhao, Z. Zhang, G. Li, H. Li, J. Wang, Z. Feng, M. Tang, X. Yuan, R. Zhang and Y. Du, *Electrochim. Acta*, 2015, **157**, 345–350; (b) J. Xu, G. Liu, J. Li and X. Wang, *Electrochim. Acta*, 2012, **59**, 105–112; (c) A. D. Blasi, C. D’Urso, V. Baglio, V. Antonucci, A. S. Arico, R. Ornelas, F. Matteucci, G. Orozco, D. Beltran, Y. Meas and L. G. Arriaga, *J. Appl. Electrochem.*, 2009, **39**, 191–196; (d) D. Profeti, T. A. F. Lassali and P. Olivi, *J. Appl. Electrochem.*, 2006, **36**, 883–888; (e) J.–M. Hu and J.–Q. Zhang, *J. Mater. Sci.*, 2003, **38**, 705–712; (f) C. P. De Pauli and S. Trasatti, *J. Electroanal. Chem.*, 2002, **538–539**, 145–151; (g) X. Chen, G. Chen and P. L. Yue, *J. Phys. Chem. B*, 2001, **105**, 4623–4628.
3. (a) J.–J. Zhang, J.–M. Hu, J.–Q. Zhang and C.–N. Cao, *Int. J. Hydrogen Energy*, 2011, **36**, 5218–5226; (b) X.–M. Wang, J.–M. Hu and J.–Q. Zhang, *Electrochim. Acta*, 2010, **55**, 4587–4593.
4. (a) P. Serp, P. Kalck and R. Feurer, *Chem. Rev.*, 2002, **102**, 3085–3128; (b) A. C. Jones and M. L. Hitchman, *Chemical Vapour Deposition: Precursors, Processes and Applications*, RSC Publishing, Cambridge 2008; (c) R. D. L. Smith, B. Sporinova, R. D. Fagan, S. Trudel and C. P. Berlinguette, *Chem. Mater.*, 2014, **26**, 1654–1659; (d) Y. Zhao, N. M. Vargas–Barbosa, E. A.

- Hernandez–Pagan and T. E. Mallouk, *Small*, 2011, **7**, 2087–2093; (e) J. D. Blakemore, N. D. Schley, G. W. Olack, C. D. Incarvito, G. W. Brudvig and R. H. Crabtree, *Chem. Sci.*, 2011, **2**, 94–98.
5. (a) P. Chandra, N. Abe, D. Takama, K. Saito, T. Yui and M. Yagi, *ChemSusChem*, 2015, **5**, 795–799; (b) H.–S. Oh, H. N. Nong, T. Reier, M. Gliech and P. Strasser, *Chem. Sci.*, 2015, **6**, 3321–3328; (c) P. E. Karthik, K. A. Raja, S. S. Kumar, K. L. N. Phani, Y. Liu, S.–X. Guo, J. Zhang and A. M. Bond, *RSC Adv.*, 2015, **5**, 3196–3199; (d) M.–C. Chuang and J.–a. A. Ho, *RSC Adv.*, 2012, **2**, 4092–4096; (e) A. Minguzzi, F.–R. F. Fan, A. Vertova, S. Rondinini and A. J. Bard, *Chem. Sci.*, 2012, **3**, 217–229; (f) T. Nakagawa, N. S. Bjorge and R. W. Murray, *J. Am. Chem. Soc.*, 2009, **131**, 15578–15579; (g) T. Nakagawa, C. A. Beasley and R. W. Murray, *J. Phys. Chem. C*, 2009, **113**, 12958–12961; (h) T. Kuwabara, E. Tomita, S. Sakita, D. Hasegawa, K. Sone and M. Yagi, *J. Phys. Chem. C*, 2008, **112**, 3774–3779; (i) M. Yagi, E. Tomita, S. Sakita, T. Kuwabara and K. Nagai, *J. Phys. Chem. B*, 2005, **109**, 21489–21491.
 6. (a) J. S. Ricci, T. F. Koetzle, M.–J. Fernandez, P. M. Maitlis and J. C. Green, *J. Organomet. Chem.*, 1986, **299**, 383–389; (b) M.–J. Fernandez and P. M. Maitlis, *J. Chem. Soc. Dalton Trans.*, 1984, 2063–2066.
 7. (a) H. N. Nong, H.–S. Oh, T. Reier, E. Willinger, M.–G. Willinger, V. Petkov, D. Teschner and P. Strasser, *Angew. Chem. Int. Ed.*, 2015, **54**, 2975–2979; (b) H. N. Nong, L. Gan, E. Willinger, D. Teschner and P. Strasser, *Chem. Sci.*, 2014, **5**, 2955–2963; (c) E. N. El Sawy and V. I. Birss, *J. Mater. Chem.*, 2009, **19**, 8244–8252.
 8. J. F. Moulder, W. F. Stickle, P. E. Sobol and K. D. Bomben, *Handbook of X-ray Photoelectron Spectroscopy*, Physical Electronics, Inc., Minnesota 1995.

9. (a) F. Li, L. Li, L. Tong, Q. Daniel, M. Göthelid and L. Sun, *Chem. Commun.*, 2014, **50**, 13948–13951; (b) M. Sharp, M. Petersson and K. Edström, *J. Electroanal. Chem.*, 1979, **95**, 123–130.
10. P. Steegstra, M. Busch, I. Panas and E. Ahlberg, *J. Phys. Chem. C*, 2013, **117**, 20975–20981.
11. (a) J. Xu, D. Aili, Q. Li, E. Christensen, J. O. Jensen, W. Zhang, M. K. Hansen, G. Liu, X. Wang and N. J. Bjerrum, *Energy Environ. Sci.*, 2014, **7**, 820–830; (b) A. A. F. Grupioni, E. Arashiro and T. A. F. Lassali, *Electrochim. Acta*, 2002, **48**, 407–418; (c) S. Fierro, A. Kapałka and C. Comninellis, *Electrochem. Commun.*, 2010, **12**, 172–174; (d) S. Fierro, L. Ouattara, E. H. Calderon and C. Comninellis, *Electrochem. Commun.*, 2008, **10**, 955–959; (e) L. M. Da Silva, J. F. C. Boodts and L. A. De Faria, *Electrochim. Acta*, 2001, **46**, 1369–1375.

CHAPTER 4

CONCLUDING REMARKS

In this dissertation, the author has succeeded in synthesis and selection suitable MOCVD precursors to deposit metal and metal-based thin film for specific applications. Two examples were given. The first one is the synthesis of a novel Ni MOCVD precursor to form high purity Ni thin films using N_2 as carrier gas. The second one is the selection of an iridium complex with Ir-Si direct bond as a MOCVD precursor to deposit an Ir oxide-doped Si oxide thin film as a highly active and stable water oxidation catalyst in acidic regime.

Chapter 2

In this chapter, a novel zero-valent Ni complex was designed and synthesized successfully. The complex possesses high vapor pressure with good thermal properties that is suitable for MOCVD. This is the first example of Ni MOCVD precursors that are able to deposit highly pure Ni film using N_2 as the carrier gas. The complex can be synthesized in high yield from commercial-available reagents, providing a prospect for scaling up for industrial application. The author hopes that this complex will be a promising Ni MOCVD precursor in future.

Chapter 3

In this chapter, the author has attempted to utilize MOCVD method to dope Si oxide into Ir oxide. An amorphous Si oxide-doped Ir oxide film was obtained by MOCVD using an Iridium complex with Ir-Si direct bonds as precursor. The film

functions as a highly active and stable water oxidation catalyst in acidic regime. This is the first example of doping Si oxide into Ir oxide to reduce Ir contents as well as to enhance catalytic activity and stability for water oxidation in acidic media. The author believes the analogous organometallic compounds with direct metal-silyl bonds will be promising single MOCVD precursors that are able to form highly homogeneous Si oxide-doped metal oxide film for applications

This work demonstrated that the MOCVD is a novel thin film preparation method. This technique not only can form pure metal film but also be able to deposit self-doping material by using a binuclear complex as single source precursor. The author believes that MOCVD will be a particularly convenient technique for the exploration and development of new functional materials in future.

Publications

Chapter 2

An N₂-compatible Ni⁰ metal-organic chemical vapor deposition (MOCVD) precursor

Viet-Ha Tran, Takeshi Yatabe, Takahiro Matsumoto, Hidetaka Nakai, Kazuharu Suzuki, Takao Enomoto and Seiji Ogo
Chem. Lett. **2015**, 44, 794-796

Chapter 3

An IrSi oxide film as highly active water-oxidation catalyst in acidic media

Viet-Ha Tran, Takeshi Yatabe, Takahiro Matsumoto, Hidetaka Nakai, Kazuharu Suzuki, Takao Enomoto, Takashi Hibino, Kenji Kaneko and Seiji Ogo
Chem. Commun. **2015**, in press (DOI: 10.1039/c5cc04286k)

ACKNOWLEDGEMENTS

I would like to express my most sincere gratitude to my supervisor Professor **Seiji Ogo** for his continuous support, supervision and encouragement during the past 3 years of my doctoral course.

I would like to appreciate Professor **Yoshio Hisaeda** and Professor **Masahiro Goto** for their evaluation of the manuscript, valuable comments and helpful advice.

I wish to thank Associate Professor **Hidetaka Nakai** for his guidance and continuously encouragement.

A special thank to Associate Professor **Ki-Seok Yoon**, Dr. **Masatatsu Suzuki** and Dr. **Kiyoshi Isobe** for their encouragement.

I am grateful to Associate Professor **Takahiro Matsumoto** and Assistant Professor **Takeshi Yatabe** for their encouragement, guidance of experiment and revising the papers.

I wish to thank Professor **Kenji Kaneko** and Professor **Takashi Hibino** for their discussion and collaboration.

I would like to thank **Tanaka Kikinzoku Kogyo** for cooperation and support, especially the advice, discussion and encouragement from Dr. **Takao Enomoto** and Dr. **Kazuharu Suzuki**.

I would like to thank Ms. **Yukiko Shigematsu** for her kind assistance and encouragement.

I thank all Ogo laboratory members for their help and sharing.

I would acknowledge **ASSURAN** International Scholarship Foundation for generous financial support and encouragement.

Finally, I thank my parents, family and friends for their unconditional love and support. Last but not least, thanks to my wife and sons who always beside and gives me love and the motivation to move forward.

Tran Viet Ha